

Design of Linear Hydrostatic Bearings

Christoph Brüner

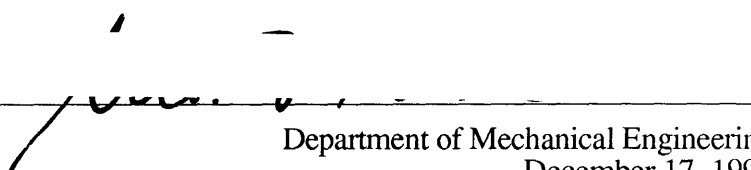
Submitted to the Department of Mechanical Engineering
in Partial Fulfillment of the Requirements for the Degree of

Master of Science

at the
Massachusetts Institute of Technology

December 1993

Signature of Author



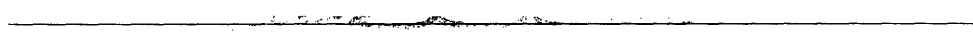
Department of Mechanical Engineering
December 17, 1993

Certified by

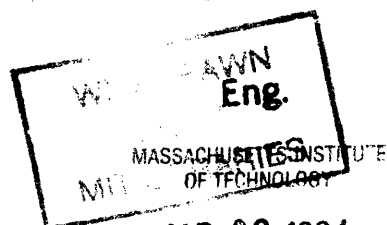


Professor Alexander H. Slocum
Thesis Supervisor

Accepted by



Professor Ain A. Sonin
Chairman, Graduate Committee



Design of Linear Hydrostatic Bearings

Christoph Brüner

Submitted to the Department of Mechanical Engineering
in Partial Fulfillment of the Requirements for the Degree of Master of Science

Abstract

New materials and the ever increasing demand for higher precision place new demands in machine tool technology. New concepts are required with much greater dimensional and thermal stability as well as improved reliability and life span. Bearing technology is a critical factor in machine tools, since they determine the machine's performance to a large extent. One possible solution in bearing technology is the use of hydrostatic bearings. They provide the necessary high damping and stiffness as well as the robustness against contamination with submicron dust particles generated during processes.

This thesis analyses and compares different kind of hydrostatic bearings for linear motion applications distinguished by the kind of flow restrictor used. Self-compensated bearings are discussed in detail and a new type of hydrostatic bearing, called Hydroguide™ is presented that overcomes the disadvantages normally associated with this type of bearing. It reduces the influence of manufacturing errors on stiffness and load capacity, has no need for hand-tuning and has no small diameter passages and therefore does not clog. The bearing uses water as working fluid, which allows for higher performance, and is environmentally friendly. The bearings thermal performance is improved by reducing the necessary pump power, and a greater heat capacity of water compared with normally used low-viscosity oil.

The fluid mechanics theory governing hydrostatic bearings is explained and formulas for the performance measures are derived. Since the Hydroguide™ is deterministic the performance can accurately be predicted using a spreadsheet. Analytical studies are performed showing the influence of different design parameters. Based on these studies design rules for different applications are determined.

The advantages of this type of hydrostatic bearing are shown in two prototypes. Experiments were conducted verifying the theory. The results present performance measures, introducing capabilities and limitations of the bearing.

Thesis Supervisor: Dr. Alexander Slocum
Title: Associate Professor of Mechanical Engineering

Konstruktion Hydrostatischer Linearführungen

Christoph Brüner

Abstract

Neue Materialien und die immer steigende Nachfrage nach Präzision erfordert neue Werkzeugmaschinentechologien. Neue Konzepte mit höherer dimensionaler und thermischer Stabilität sind erforderlich bei gleichzeitig verbesserter Zuverlässigkeit und erhöhter Lebensdauer. Führungselemente sind ein kritisches Element im Werkzeugmaschinenbau, da sie zu einem großen Teil die Genauigkeit der Maschine bestimmen. Eine mögliche Lösung in der Führungstechnik ist die Anwendung von hydrostatischen Lagern. Sie verfügen sowohl über hervorragende Dämpfungseigenschaften, und haben eine hohe Steifigkeit als auch die notwendige Robustheit gegen Verschmutzung mit Staubteilchen kleiner als ein Mikron, die während der Bearbeitungsprozesse entstehen.

Diese Arbeit analysiert unterschiedliche Arten hydrostatischer Linearführungen unterschieden nach der Art des Vorwiderstandes. Hydrostatische Lager mit Laufspaltdrossel werden im Detail behandelt und ein neues Lager, Hydroguide™, vorgestellt das die normalerweise mit dieser Art der Lagerung verbundenen Nachteile verringert. Es vermindert den Einfluß von Fertigungsungenauigkeiten auf die Steifigkeit und Nachgiebigkeit, benötigt keine Nacharbeit und Feineinstellung der Vorwiderstände und die Verstopfungsgefahr ist gering da keine Zulaufbohrungen mit kleinen Durchmesser benötigt werden. Die Verwendung von Wasser als Schmiermittel ermöglicht eine höhere Leistung und macht das Lager umweltfreundlich. Die thermische Leistung des Lagers wird verbessert durch eine verringerte notwendige Pumpenleistung und die höhere Wärmekapazität von Wasser im Vergleich zu den normalerweise verwendeten Ölen.

Die Störungsmechaniktheorie die das Verhalten des Lagers beschreibt ist erklärt und das Lager beschreibende Formeln abgeleitet. Da das Hydroguide™ Lager deterministisch ist die kann die Leistung, mit Hilfe von einfachen Computerprogrammen präzise vorausgesagt werden. Die Ergebnisse wurden in ein Tabellenkalkulationsprogramm implementiert. Analytische Studien wurden durchgeführt, die den Einfluß verschiedener Konstruktionsparameter verdeutlichen. Aufbauend auf den Studien wurden Konstruktionsregeln für verschiedene Anwendungsfälle aufgestellt.

Die Vorteile dieses Lagers wird in zwei Hydroguide™ Prototypen aufgezeigt. Experimente wurden durchgeführt die die Theorie verifizieren. Die Ergebnisse beschreiben die Leistung und die Grenzen dieses Lagers.

Acknowledgments

I would like to thank Professor Alexander Slocum. For all the inspiration and all things I learned during my studies at MIT.

I am entirely thankful to Heinz Gaub for his never ending support and his friendship.

Contents

List of Figures

1. Introduction	10
1.1 Background	10
1.2 Statement of Objective	11
1.3 Thesis Layout	11
2. Theory on Hydrostatic Bearings	12
2.1 Operating Principle	12
3. Analysis of Linear Hydrostatic Bearings	14
3.1 Static and Dynamic Behavior	18
3.1.1 Fluid Mechanic Theory	18
3.1.2 Resistances	23
3.1.3 Effective Bearing Pad Area	26
3.1.4 Fluid Flow Rates and Fluid Velocities	27
3.1.5 Load capacity	27
3.1.6 Stiffness	28
3.1.7 Damping	28
3.2 Thermal Behavior	29
3.3 Design of Flow Restrictors	32
3.3.1 Constant flow devices	32
3.3.2 Laminar flow devices with fixed compensation	32
3.3.3 Laminar flow devices with variable compensation	33
3.3.4 Laminar flow devices with self-compensation	33
4. Comparison of Self- and Fixed-Compensated Hydrostatic Bearings	39
4.1 Load Capacity and Stiffness	39
4.2 Manufacturing Error	42
4.3 System Design	44
5 Case Study 1: Low Pressure Bearing	48
5.1 Design Considerations	48
5.2 Manufacturing	50
5.3 Bearing Design	51
5.4 Measurements	53
5.3.1 Straightness	53
5.3.2 Stiffness and Dynamic Response	58

6. Case Study 2: High Pressure Bearing	62
6.1 Design Considerations	62
6.2 Manufacturing	64
6.3 Bearing design	64
7. Conclusion	68
8. References	69
9. Appendices	
9.1 Appendix A: Spreadsheet for Case Study 2	70
9.2 Appendix B: Mechanical Drawings for Case Study 2	75
9.3 Appendix C: Spreadsheet for Case Study 2	78
9.4 Appendix D: Mechanical Drawings for Case Study 2	83

List of Figures

- Figure 3.1: Stiffness and damping of a machine tool carriage.
- Figure 3.2: Bearing model and electrical circuit analogy.
- Figure 3.3: Fluid velocity profiles in hydrostatic bearing gaps.
- Figure 3.4: Fluid velocity profiles in hydrostatic bearing gaps.
- Figure 3.5: Fluid velocity profiles in hydrostatic bearing gaps.
- Figure 3.6: Bearing pocket geometry.
- Figure 3.7: Squeeze film between two parallel plates.
- Figure 3.8: Total power and power factor K for changing nominal gap.
- Figure 3.9: Flat-edge-pin: Laminar flow devices with fixed compensation.
- Figure 3.10: Variable compensation device (Diaphragm-Type).
- Figure 3.11: Bearing pad and restrictor pad geometry.
- Figure 3.12: The principle of self-Compensation using Hydroguide™.
- Figure 3.13: Load capacity of a self-compensated hydrostatic bearing.
- Figure 3.14: Stiffness of a self-compensated hydrostatic bearing.
- Figure 4.1: Load capacity of a fixed-compensated hydrostatic bearing.
- Figure 4.2: Load capacity of a self-compensated hydrostatic bearing (Hydroguide™).
- Figure 4.3: Stiffness of a fixed-compensated hydrostatic bearing.
- Figure 4.4: Stiffness of a self-compensated hydrostatic bearing (Hydroguide™).
- Figure 4.5: Manufacturing error of a fixed-compensated hydrostatic bearing.
- Figure 4.6: Manufacturing error of a self-compensated hydrostatic bearing.
- Figure. 5.1: Schematic of the hydrostatic bearing design using bearing blocks.
- Figure. 5.2: Low pressure hydrostatic test bearing.
- Figure. 5.3: Bending moment on bearing blocks.
- Figure. 5.4: Load capacity of the low pressure test bearing.
- Figure. 5.5: Stiffness of the low pressure test bearing.
- Figure. 5.6: Noise floor of the laser measurement system.
- Figure. 5.7: Error motion of the carriage with 20 psi supply y pressure.
- Figure. 5.8: Straightness (250 mm) plot of granite bearing.
- Figure. 5.9: The spectral components of the carriage's straightness error.
- Figure. 5.10: Straightness (100 mm) plot of granite bearing.
- Figure 5.11: Noise level during straightness measurement.
- Figure 5.12: Bearing pocket pressure as a function of supply pressure.
- Figure 5.13: Bearing pocket pressure as a function of supply pressure.

- Figure 5.14: Dynamic response of the carriage with supply pressure on and off.
- Figure 6.1: Bearing arrangement (wrap-around) of case study 2.
- Figure 6.2: Ceramic test bearing.
- Figure 6.3: Load capacity of the high pressure bearing.
- Figure 6.4: Stiffness of the high pressure bearing.
- Figure 6.5: Total power as a function of supply pressure.
- Figure 6.6: Stiffness at zero displacement as a function of supply pressure.
- Figure 7.1: Properties of a self-compensated bearing.

List of Variables

A_{eff} :	Effective bearing area	$[\text{m}^2]$
c	Specific heat capacity	$[\text{J}/\text{kg K}]$
F :	Load Capacity	$[\text{N}]$
h :	nominal bearing gap	$[\text{m}, \mu\text{m}]$
K :	Stiffness	$[\text{N}/\mu\text{m}]$
P_f :	Friction power	$[\text{W}]$
P_p :	Pump power	$[\text{W}]$
P :	Pressure	$[\text{Pa}=\text{N}/\text{m}^2]$
p_s :	Supply pressure	$[\text{Pa}=\text{N}/\text{m}^2]$
Δp :	Pressure difference between upper and lower bearing pad	$[\text{Pa}=\text{N}/\text{m}^2]$
Q :	Fluid flow	$[\text{l}/\text{min}]$
R :	Resistance	$[\text{Nsec}/\text{m}^5]$
R_{ur} :	Resistance of upper restrictor pad	$[\text{Nsec}/\text{m}^5]$
R_{lr} :	Resistance of lower restrictor pad	$[\text{Nsec}/\text{m}^5]$
R_{ub} :	Resistance of upper bearing pad	$[\text{Nsec}/\text{m}^5]$
R_{lb} :	Resistance of lower bearing pad	$[\text{Nsec}/\text{m}^5]$
v :	Fluid velocity	$[\text{m}/\text{sec}]$
γ :	Restrictor resistance to bearing resistance ratio	
μ :	Dynamic viscosity	$[\text{Nsec}/\text{m}^2]$
ν :	Kinematik viscosity	$[\text{m}^2/\text{sec}]$
ρ :	Density	$[\text{kg}/\text{m}^3]$
δ :	Displacement	$[\text{m}, \mu\text{m}]$
τ :	Fluid shear stress	$[\text{N}/\text{mm}^2]$

1. Introduction

Linear and angular bearing technology is a critical factor in machine tools, since they determine the machine's performance to a large extent. They have to guide the relative moving workpiece and tool with a high degree of accuracy repeatable over time. To minimize the error motions introduced by bearings they must provide superior performance in terms of stiffness, load capacity and damping as well as motion resolution. In addition, bearings contribute considerably to the machine's manufacturing cost.

In most machine tool applications rolling element or hydrodynamic bearings are used. Hydrostatic bearings provide the superior performance characteristics that are desired, but are not widely used because of several disadvantages generally associated with this type of bearing. They require expensive support equipment, such as pumps, filters, and collection systems and are therefore expensive. Furthermore they need careful monitoring and maintenance for reliable operation. The design relies mostly on experience, since their performance can not be predicted accurately and for that reason a considerable amount of hand-tuning is necessary during assembly.

However, a new type of hydrostatic bearing was developed that overcomes most of these disadvantages. It requires lower flow rates, therefore smaller pumps and hence generates less heat. It is less sensitive to manufacturing errors, requires no hand-tuning, uses water instead of oil as working fluid and is deterministic. The bearing's performance is described by simple equations and can be predicted accurately.

1.1 Background

New materials and the ever increasing demand for higher precision place new demands in machine tool technology. E.g. manufacturing ceramics economically with a high degree of accuracy is one of the challenges for future machine tool technology, since they require machines with much greater dimensional and thermal stability. In addition, the durability of machines has to be improved. Since ceramic particles of submicron size are produced during the process that wear seals and ultimately damage slide-way and spindle bearings, particularly rolling element bearings.

One possible solution in bearing technology is the use of hydrostatic bearings. They provide the necessary high damping and stiffness as well as the robustness against contam-

ination with ceramic dust. The new self-compensated hydrostatic bearing presented fits these needs.

1.2 Statement of Objective

This thesis analyses and compares different kind of hydrostatic bearings distinguished by the kind of flow restrictor used. Self-compensated bearings are discussed and a new type of hydrostatic bearing, called Hydroguide™ is presented that overcomes the disadvantages normally associated with this type of bearing. Design rules are derived and solutions are introduced that show the implementation of the theory. Performance measures are provided, that show the capabilities and limitations of the bearing. This thesis can be used as a guideline comparing the Hydroguide™ to other bearings and to guide a design of a linear motion system using Hydroguide™.

1.3 Thesis Layout

The second chapter illustrates the theory on hydrostatic bearings and explains the operating principle. Since hydrostatic bearings are distinguished by the kind of flow restrictor used, different restrictors are introduced and their advantages and disadvantages are discussed briefly. Chapter 3 derives the basic equations, that describe the mechanical and thermal behavior of hydrostatic bearings. Formulas for the most important performance measures, for instance load capacity and stiffness, are derived and implemented into a spreadsheet.

In chapter 4 different kind of flow restrictors and a new type of hydrostatic bearing called Hydroguide™ are introduced. Using the spreadsheet written, parameter studies show the performance of bearings with different restriction under varying conditions. Fixed compensated and self-compensated bearings using Hydroguide™ are compared in detail. Chapter 5 and 6 describe the application of the Hydroguide™ to linear motions, presenting two prototypes build during the course of this thesis. Design and testing are discussed in detail.

Chapter 7 completes the thesis with a summary of the conclusions drawn.

2. Theory on Hydrostatic Bearings

2.1 Operating Principle

Hydrostatic bearings utilize a thin film of externally pressurized fluid between the relative moving parts to support loads. The fluid is supplied with high pressure to bearing pockets from which it flows across lands restricted on the opposite side by the bearing rail. The distance between bearing land and rail is generally referred to as bearing gap. This gap restricts the flow out of the pocket, leading to a difference between the pocket and the ambient pressure. This differential pressure times the land area is the force that supports the load. Since pressure is distributed over a large area of several bearing pads, large loads can be supported. In order to obtain bidirectional stiffness and load capacity, the support bearing can be preloaded by means of an opposed pad, the preload bearing pad. Since this is most common in machine tool applications, this configuration will be discussed in this thesis.

As the bearing is loaded it is displaced and the load bearing gap decreases, while the preload bearing gap increases. Positive displacement δ is defined as decrease of the load bearing gap as response to a positive load. In order to realize different equilibrium positions at varying loads differential pocket pressures must be realized. This is possible by regulating the inlet-flow into the bearing pockets. Flow restrictors in series with the bearing pockets serve this purpose which is generally referred to as compensation. Without compensation the bearing would not be able to support any load. Different restrictors and advantages are discussed. With varying loads applied, the bearing displaces according to its stiffness and load capacity. Stiffness and load capacity are itself a function of the bearing gap. The influence of bearing displacement will be discussed in chapter 3.

As the bearing moves along a rail the straightness is determined by the pressure fluctuations in the supply lines, the heat generated into the system, the first order straightness of the rail and the tendency to build up a hydrodynamic wedge at higher speeds. Since the load is distributed over the bearing area, parallel and straightness errors smaller than 1/10 the bearing gap will not result in an error motion of the supported carriage.

There is very low friction in hydrostatic bearings in particular no static friction at all. At low speeds it operates without stick slip effects. The motion resolution therefore depends only on type actuators and, sensors and controllers and there will be no positioning error

introduced by the bearing using an indirect measurement system. In addition, there is no wear and if properly handled hydrostatic bearings have potentially infinite life.

Power is generated by two sources during operation and entirely dissipated as heat: The pump power and viscous shear power in the fluid introduced by the relative moving parts. The former dominates in linear motion systems, due to generally low speeds (v_{\max} ca. 30m/min for a surface grinding table). The pump power is the product of pressure and flow. Assuming a fixed pressure for a desired load capacity, reducing the flow is the best mean of reducing the power introduced into the system.

Hydrostatic bearings normally use oil as working fluid (e.g. ISO 10 oil with $\mu=0.01$ Nsec/m²). Oil has desired properties, it is an excellent lubricant and long term stable, but its viscosity is high and its heat capacity is low. High load capacity and stiffness require small bearing gaps. With smaller bearing gaps the resistance increases and lower viscosity fluid are desirable to reduce the vicious shear generated due to the high resistance. Water has one tenth of the viscosity of low viscosity oil and four times the heat capacity. Water decreases the power generated and transferred into the system, provides higher performance and is environmentally friendly.

3. Analysis of Linear Hydrostatic Bearings

The force exerted on the fluid film against the rail and the carriage must, by equilibrium, balance the applied bearing load. The response of the machine to these forces depends on its stiffness, damping and its mass. Stiffness and damping are each necessary, but individually not sufficient for a precision machine. Damping in hydrostatic bearings depends on the velocity of the carriage with respect to the base. Thus, the bearing may not be much stiffer than the machine structure, because very little damping in the bearing would occur. Bearings are critical elements in the structural loop of the machine, since their static and dynamic behavior has a significant influence on the overall response.

In a machine tool as shown in Figure 3.1 the importance of bearing technology to the overall performance and the influence of stiffness k and damping factor c of a linear guide can also be interpreted in terms of workpiece accuracy. As the static force displaces the carriage with respect to the tool errors are introduced, which result in shape inaccuracy. Damping dissipates the energy generated by vibrations. The less damping is provided and therefore the less energy is dissipated by the bearing the larger are the responding error motions of the carriage with respect to the structure. The damping factor determines the surface finish of the workpiece to a large extent. Hydrostatic bearings comply with these high demands and their performance can be analyzed and predicted using a simple fluid model

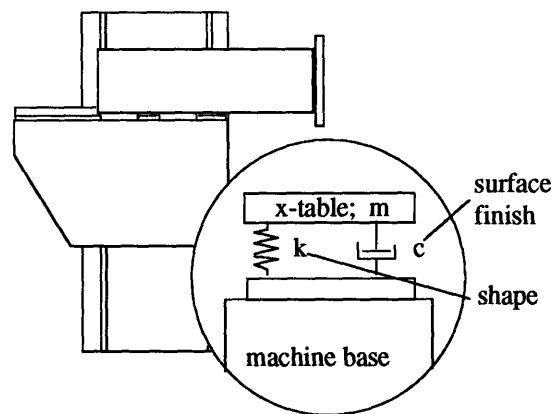


Figure 3.1: Stiffness and damping of a machine tool carriage.

In order to support bidirectional load most applications of hydrostatic bearings are preloaded by means of an opposed pad configuration. This configuration is analyzed using the law of Hagen-Poussuille $P=QR$, in analogy to the law of Ohm for electrical circuits. A

pressure source and four restrictors are used to model the hydrostatic bearing. R_l and R_p are the load and preload bearing pad resistances, while the resistances at the entrance to the bearings provide a means of regulating the flow and therefore establishing a differential pressure between the upper and the lower bearing pad. These are generally referred to as restrictor resistances or compensation. Figure 3.2 shows the bearing model and the electrical circuit analogy for the opposed pad hydrostatic bearing.

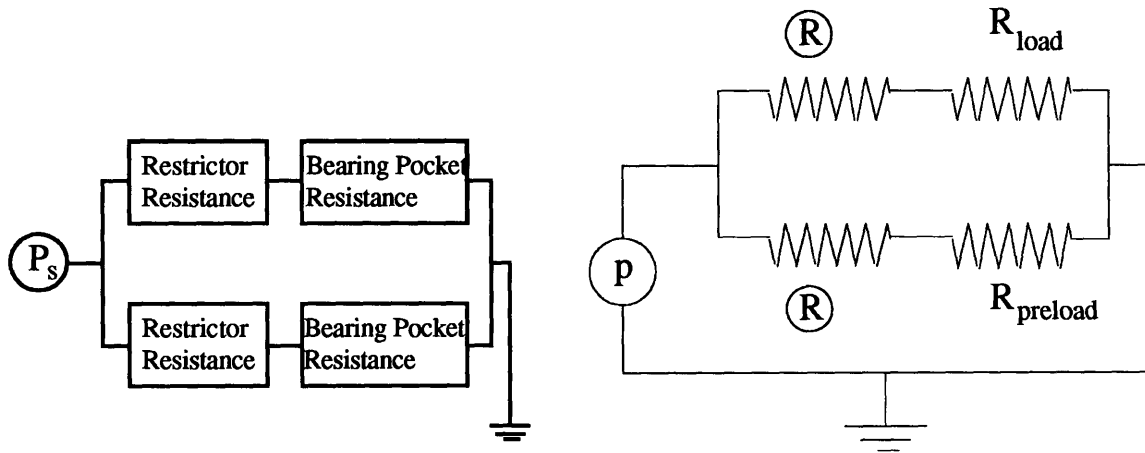


Figure 3.2: Bearing model and electrical circuit analogy.

Using this model the nominal total fluid flow resistance of the undisplaced opposed pad hydrostatic bearing, modeled from two resistances in parallel each consisting of two resistances in series, is

$$R = \frac{1}{\frac{1}{R + R_l} + \frac{1}{R + R_p}} \quad (3.1)$$

This leads to the pocket pressure and the pressure difference in the load and preload bearing pad. The pocket pressure in the load bearing is

$$p_l = p_s \left(\frac{R_l}{R + R_l} \right) \quad (3.2)$$

The pocket pressure in the preload bearing is

$$p_p = p_s \left(\frac{R_p}{R + R_p} \right) \quad (3.3)$$

The pressure difference is thus

$$\Delta p = p_l - p_p = p_s \left(\frac{R_l}{R + R_l} - \frac{R_p}{R + R_p} \right) \quad (3.4)$$

As seen in equation (3.4) for zero as well as infinite restrictor resistances the bearing is not able to support a load since the differential pressure between the opposed bearing pad equals zero. The ideal resistance for maximized differential pressure is found by taking the partial derivative of the pressure difference with respect to the restrictor resistance. Assuming that $\delta \ll h$ we can neglect all non linear δ -terms the ideal restrictor resistance for the fluid circuit that balances the resistance bridge is

$$R_{ideal} = \frac{\gamma}{h^3}, \text{ with } \gamma = \frac{R_{restrictor}}{R_{bearing}} \quad (3.5)$$

Thus, the pocket pressure for a changing bearing gap, i.e. under displacement δ can be determined. The pressure in the load bearing pocket under displacement δ is

$$p_l = p_s \left(\frac{h^3}{(h - \delta)^3 + h^3} \right) \quad (3.6)$$

and the pressure in the preload bearing pocket is

$$p_p = p_s \left(\frac{h^3}{(h + \delta)^3 + h^3} \right) \quad (3.7)$$

The pressure difference between the load and preload bearing pad in an opposed bearing configuration under a displacement δ is thus

$$\Delta p = p_l - p_p = p_s h^3 \left(\frac{1}{(h - \delta)^3 + h^3} - \frac{1}{(h + \delta)^3 + h^3} \right) \quad (3.8)$$

Again, it is obvious that at zero displacement both pocket pressure are equal and the resulting pressure difference is zero.

3.1 Static and Dynamic Behavior

The static and dynamic behavior of hydrostatic bearings is determined by the properties of the fluid film. As shown in the following chapter, the pressure distribution in the bearing pads can be analytically determined. The load that can be supported by the bearing is therefore the sum of the products of pressure times the area of several elements of the bearing geometry. A typical geometry of a hydrostatic bearing pad is shown in Figure 3.6 For the analysis the bearing is divided into regions analyzed by using different forms of the Navier-Stokes equation.

As seen earlier, it is possible to model fluid systems in analogy to electric circuit systems. In the same way the law of Hagen-Poiseuille corresponds to the law of Ohm, the rules for electrical resistances in parallel and series apply for fluid resistances. To be able to model the entire bearing system the resistances have to be determined first.

3.1.1 Fluid Mechanic Theory

The knowledge of pressure distribution in the bearing pocket is essential for the derivation of equations describing the behavior of hydrostatic bearings. Assuming a laminar, viscous flow between two parallel plates the Navier-Stokes equation is applied describing the motion of the fluid [12]. This differential equation of motion of a viscous fluid is very difficult to apply, but analytical solutions can be obtained for a few simple flows. Fortunately, the flow in the bearing pads can be modeled obtaining simple solutions. Considering steady flow with a velocity field depending only on two spatial dimensions and choosing appropriately simple boundary conditions.

To describe the flow in different bearing geometries it is necessary to express solution in the cartesian as well as the polar form of the Navier-Stokes equation for an incompressible fluid with constant viscosity. The general form of the Navier-Stokes equation is

$$\frac{DV}{Dt} = -\frac{1}{\rho} \nabla p + g + \nu \nabla^2 V \quad (3.9)$$

with $(1/\rho)\nabla p$, g , $\nu \nabla^2 V$ the pressure force, the gravity force and the viscous force per unit mass respectively. The principle of solving the Navier-Stokes equation is shown

for the cartesian form demonstrating the underlying fluid mechanics. The same principle applies for the polar form for which solutions are derived as well.

In the case of hydrostatic bearings, fluid flows through narrow channels by means of a pressure difference and an additional velocity component introduced by the carriage moving at a constant speed V . For both cases the fluid profile, the flow rate and the resulting pressure distribution can be determined separately. The flows are generally referred to as 'Plane Couette Flow' and 'Plane Poiseuille Flow' respectively.

In the case of 'Plane Poiseuille Flow' the flow is restricted by two fixed parallel plates separated by a distance h , the bearing gap. For hydrostatic bearings this corresponds to a carriage sitting stationary. The following assumptions can be made: the pressure gradient is constant in x -direction, a positive fluid velocity V in the x -direction as a function of y , and all remaining velocity components zero. Thus, substituting these assumptions the cartesian Navier-Stokes equation is reduced to

$$0 = -\frac{1}{\rho} \frac{\partial p}{\partial x} + \nu \left(\frac{\partial^2 u}{\partial y^2} \right) \quad (3.10)$$

Note that u and p depend only upon y and x respectively, and thus by integrating twice and applying the boundary conditions of zero velocity on the walls, $u(0)=0$ and $u(h)=0$, the constants of integration can be determined and the velocity profile $u(y)$ is found

$$u = \frac{1}{2\rho\nu} \frac{\partial p}{\partial x} (y^2 - yh) \quad (3.11)$$

$$u_{\max} = \frac{h^2}{8\mu} \left(-\frac{\partial p}{\partial x} \right), \text{ at } y=h/2 \quad (3.12)$$

This flow is parabolic with the maximum velocity (u_{\max}) at the center of the channel as shown in Figure 3.3.

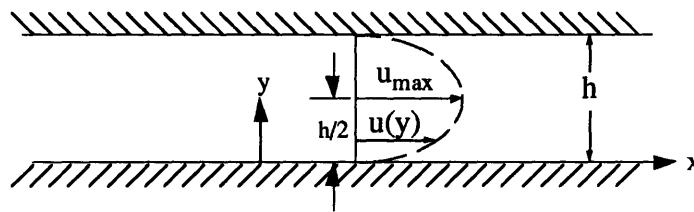


Figure 3.3: Fluid velocity profiles in hydrostatic bearing gaps.

The flow rate through a cross section of area dh , where d is the depth of the parallel plates, is found by integrating twice across h

$$Q = \int_0^h u dA = \frac{1}{2\mu} \left(-\frac{\partial p}{\partial x} \right) \int_0^d \int_0^h y(h-y) dy dz \quad (3.13)$$

$$Q = \frac{d}{2\mu} \left(-\frac{\partial p}{\partial x} \right) \cdot \left[\frac{y^2 h}{2} - \frac{y^3}{3} \right]_0^h \quad (3.14)$$

$$Q = \frac{dh^3}{12\mu} \left(-\frac{\partial p}{\partial x} \right) \quad (3.15)$$

Thus, we can determine the pressure distribution of the laminar, viscous flow in the gap due to a differential pressure. The x -dimension, in the case of the hydrostatic bearings, is called land width l . Integration across l in x direction therefore yields

$$\int_{p_1}^{p_2} dp = \frac{-12\mu Q}{dh^3} \int_0^l dx \quad (3.16)$$

$$p_2 - p_1 = \frac{-12l\mu}{dh^3} Q \quad (3.17)$$

$$\Delta p = \frac{-12l\mu}{dh^3} Q \quad (3.18)$$

Assuming, that the pressure p_1 is atmospheric pressure, Δp is the gage pressure along the bearing land width l . In most applications the atmospheric pressure is assumed to be zero and the equation reduces to

$$p_1 = \frac{12l\mu}{dh^3} Q \quad (3.19)$$

The same analysis applies to the polar form of the Navier-Stokes equation in order to determine the pressure distribution for rounded parts of the bearing pad. Again, assuming Plane Poiseuille Flow the polar Navier-Stokes equation reduces to

$$\frac{1}{\mu} \frac{\partial p}{\partial r} = \frac{\partial^2 u}{\partial z^2} \quad (3.20)$$

By integrating twice and applying the boundary conditions of zero velocity on the walls $u(z=0)=0$ and $u(z=h)=0$, the constants of integration can be determined and the velocity profile is found

$$u = \frac{1}{2\mu} \frac{\partial p}{\partial r} (z^2 - zh) \quad (3.21)$$

The flow rate out of a full annulus is found

$$Q = \int_0^h u dA = \frac{1}{2\mu} \left(-\frac{\partial p}{\partial r} \right) \int_0^{2\pi} \int_0^h (zh - z^2) dz d\theta \quad (3.22)$$

$$Q = \frac{\pi h^3 r}{6\mu} \left(-\frac{\partial p}{\partial r} \right) \quad (3.23)$$

Thus, we can determine the pressure distribution by integration across l in r direction, with r_p the inner radius and l the land width as shown in Figure 3.6.

$$\int_{p_1}^{p_2} dp = \frac{-6\mu Q}{\pi h^3} \int_{r_p}^{r_p+l} \frac{dr}{r} \quad (3.24)$$

And the pressure for a full annulus distribution is found

$$\Delta p = \frac{6\mu \log_e \left(\frac{r_p + l}{r_p} \right)}{\pi h^3} Q \quad (3.25)$$

Steady viscous Plane Couette Flow exists when one of the parallel plates moves at a constant speed V_p in x direction, that depends on y only. Since there is no pressure difference between the inlet and the outlet, there is no pressure change imposed on the flow. The velocity along a streamline is constant so that the material derivative DV/Dt equals zero. Noting that only y derivatives are non zero the Navier-Stokes equation reduces to

$$0 = \nu \frac{\partial^2 u}{\partial y^2} \quad (3.26)$$

$$\frac{\partial^2 u}{\partial y^2} = 0 \quad (3.27)$$

Integrating twice and determining the constants of integration by applying the boundary conditions $u(y=0)=0$ and $u(y=h)=V_p$ yields the velocity profile as shown in Figure 3.4.

$$u = V_p \left(\frac{y}{h} \right) \quad (3.28)$$

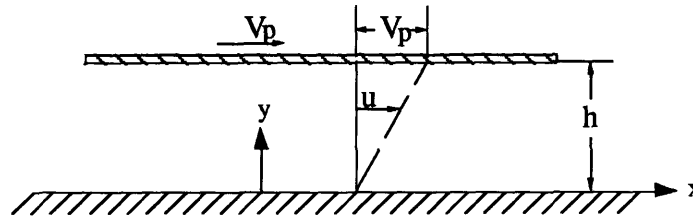


Figure 3.4: Fluid velocity profiles in hydrostatic bearing gaps.

The flow rate in x-direction through a cross section of area bh , introduced by the moving plate is found by integrating twice across h

$$Q = \iint V dA = d \int u dy = \frac{d * V_p}{h} \frac{y^2}{2} \Big|_0^h \quad (3.29)$$

$$Q = \frac{1}{2} d V_p h \quad (3.30)$$

It should be noted, that for the calculation on hydrostatic bearings the latter is of minor importance, because even in the case of a moving carriage when the pressure distribution changes the net pressure across the bearing pad basically remains unchanged. Therefore the basis of the bearing calculations is the pressure distribution due to Plane Poisseuille flow. But it is important to know the total fluid velocity and the total fluid flow rate in order to determine a condition for the maximum carriage velocity. As a general rule the flow rate due to the pressure difference should be on the order twice that due to the flow dragged into the bearing by relative motion. The maximum speed of the carriage supported by a bearing with $\gamma=1$ and the smallest pocket pressure p is

$$v_{\max} = \frac{ph^2}{12l\mu} \quad (3.31)$$

The Navier-Stokes equation for both flows is linear and thus the resulting flow can be attained by superposition. The combined fluid velocity profile due to a moving plate and a constant non zero pressure gradient is shown in Figure 3.5.

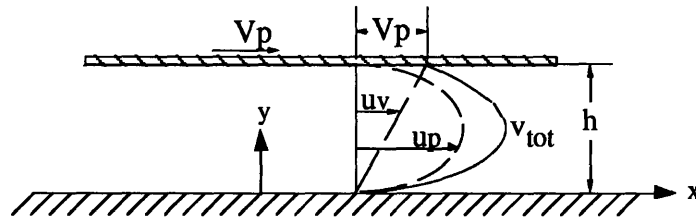


Figure 3.5: Fluid velocity profiles in hydrostatic bearing gaps.

3.1.2 Resistances

Applying the results from the fluid mechanics analysis according to the law of Hagen-Poussieuille $p=RQ$ the resistance for a single bearing pad can be calculated [1] [3]. Therefore the bearing pad is divided into several regions as shown in Figure 3.5 enabling an analysis using the two forms of the Navier-Stokes equation. The resistance R_s for the straight regions are taken together and described by a land width d containing all four regions. The resistance R_p for the four polar regions can be attained by deriving the solution for a complete annulus as derived before.

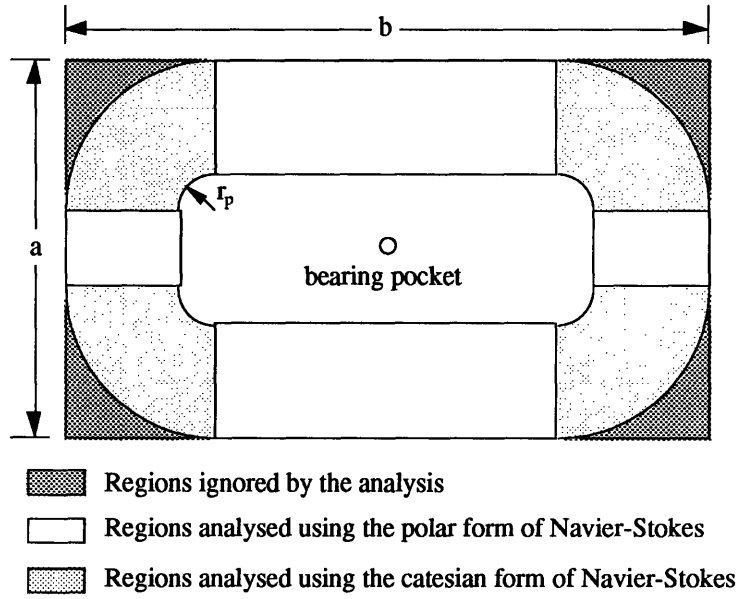


Figure 3.6: Bearing pocket geometry.

The total resistance of the rectangular bearing pocket is thus

$$R = \frac{1}{R_s} + \frac{1}{R_p} \quad (3.32)$$

and with the distance d , the theoretical depth of the straight bearing regions

$$d = 2(a + b - 4(l + r_p)) \quad (3.33)$$

the fluid resistance R_s becomes using the solution for plane Poussieulle flow as derived earlier

$$R_s = \frac{6l\mu}{(a + b - 4(l + r_p))h^3} \quad (3.34)$$

Assuming a full circle annulus the resistance R_p of the rounded regions becomes

$$R_p = \frac{6\mu \log_e \left(\frac{r_p + l}{r_p} \right)}{\pi h^3} \quad (3.35)$$

With these two resistances the total resistance of a rectangular bearing pocket is

$$R_s = \frac{6\mu}{h^3 \left(\frac{\pi}{\log_e \left(\frac{r_p + l}{r_p} \right)} + \frac{a + b - 4(l + r_p)}{l} \right)} = \frac{\gamma}{h^3} \quad (3.36)$$

The actual flow resistance of the load bearing pad under a displacement δ is

$$R_s = \frac{6\mu}{(h - \delta)^3 \left(\frac{\pi}{\log_e \left(\frac{r_p + l}{r_p} \right)} + \frac{a + b - 4(l + r_p)}{l} \right)} = \frac{\gamma}{(h - \delta)^3} \quad (3.37)$$

The actual flow resistance of the preload bearing pad under a displacement δ is

$$R_s = \frac{6\mu}{(h + \delta)^3 \left(\frac{\pi}{\log_e \left(\frac{r_p + l}{r_p} \right)} + \frac{a + b - 4(l + r_p)}{l} \right)} = \frac{\gamma}{(h + \delta)^3} \quad (3.38)$$

Assuming laminar, viscous flow the resistance of the bearing pockets is found to be a function of the pad geometry, the bearing gap and the viscosity of the fluid. Thus, as the bearing is loaded and displaced the bearing gap and therefore the bearing pads resistance changes.

3.1.3 Effective Bearing Pad Area

To determine the force exerted on the bearing pads the effective bearing pad area must be considered. The effective bearing pad area takes into account the pressure drop across the bearing lands.

The entire pocket area is

$$A_p = (a - 2l)(b - 2l) + r_p^2(\pi - 4) \quad (3.39)$$

The total land area over which viscous shear occurs in the bearing gap is

$$A_l = ab - A_p \quad (3.40)$$

For the straight land regions of Figure 3.5, the pressure decays linearly from the pocket pressure to zero, and the effective area of the straight lands is therefore half of their actual area

$$A_{sl} = l(a + b - 4(l + r_p)) \quad (3.41)$$

For the rounded regions of Figure 3.2, the pressure decays logarithmically from the pocket pressure to zero. The effective area therefore is

$$A_{rl} = \pi \left(\frac{l(2r_p + l)}{2 \ln \left(\frac{r_p + l}{r_p} \right)} - r_p^2 \right) \quad (3.42)$$

This yields a total effective bearing area of

$$A_{rl} = (a - 2l)(b - 2l) + r_p^2(\pi - 4) + l(a + b - 4(l + r_p)) \pi \left(\frac{l(2r_p + l)}{2 \ln \left(\frac{r_p + l}{r_p} \right)} - r_p^2 \right) \quad (3.43)$$

3.1.4 Fluid Flow Rates and Fluid Velocities

The total fluid flow rate for the undisplaced bearing at nominal bearing gap is

$$Q = \frac{p_s}{R} = \frac{p_s h^3}{\gamma} \quad (3.44)$$

The lowest flow velocity occurs at the outer circumferences of the bearing pad. It is the fluid flow rate out of the bearing pocket divided by the area the fluid flows through. The flow rate out of the upper bearing pad a at displacement δ is

$$Q_{ub} = \frac{p_u}{R_{ub}} \quad (3.45)$$

and the velocity of the fluid leaving the upper bearing land is

$$v_{ub} = \frac{Q_{ub}}{2(a+b)(h-\delta)} \quad (3.46)$$

The flow rate out of the lower bearing pad a at displacement δ is

$$Q_{lb} = \frac{p_l}{R_{lb}} \quad (3.47)$$

and the velocity of the fluid leaving the upper bearing land is

$$v_{lb} = \frac{Q_{lb}}{2(a+b)(h+\delta)} \quad (3.48)$$

3.1.5 Load capacity

The Load capacity is load that the bearing system can support at a given displacement δ . It is the pressure difference of the opposed bearing pockets times the effective bearing area. Since it is a function of the supply pressure and the area of the bearing pads it can easily be increased by increasing the two variables.

$$F = A_{eff} \Delta p = p_s A_{eff} h^3 \left[\frac{1}{[(h - \delta)^3 + h^3]} - \frac{1}{[(h + \delta)^3 + h^3]} \right] \quad (3.49)$$

3.1.6 Stiffness

Stiffness is the partial derivative of the load capacity with respect to the change in bearing gap, the displacement δ .

$$K = \frac{\partial F}{\partial \delta}$$

$$K = 3p_s A_{eff} h^3 \left[\frac{(h - \delta)^2}{[(h - \delta)^3 + h^3]} + \frac{(h + \delta)^2}{[(h + \delta)^3 + h^3]} \right] \quad (3.50)$$

3.1.7 Damping

Damping in hydrostatic bearings is achieved through the energy dissipated in the fluid film. This is generally referred to as squeeze film damping. As the fluid film is forced out of the bearing gap, due to viscous effects the fluid resists this extrusion and a pressure is build up. Thus the approach is slowed down. By the action of varying loads the fluid film is not only subjected by the squeezing action but also by the absorption in each cycle. Therefore, due to the large areas of fluid film hydrostatic bearings provide excellent damping.

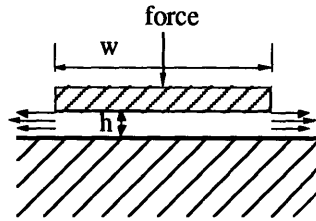


Figure 3.7: Squeeze film between two parallel plates.

Analytical solution describing the damping capability of small fluid films can be obtained, but are only rough approximations and the assumption made are not always valid. Thus, results can differ significantly for different applications. However, a simple formula as derived by Fuller [8] is helpful in gaining a better insight to the effect of squeeze film

damping. The formula is derived for two parallel, rectangular plates of width w and length l assuming two dimensional flow. The damping factor is

$$b = K_s \frac{\mu l w^3}{h^3} \quad (3.51)$$

where μ is the viscosity of the fluid and K_s a geometric factor related to the bearing. For $l/w > 10$ $K_s = 1$.

As stated before, the larger the areas the larger the damping capability. The smaller the bearing gap and the larger the viscosity, the better the damping. It should be noted, that squeeze film damping does not depend on the pocket pressure. Thus, the damping capability is the same for all types hydrostatic bearings.

It should be noted that the area of hydrostatic bearings is restricted by the application and the choice of the fluids viscosity greatly influences the bearing gap chosen. Therefore a trade off between the desirable fluid qualities and the damping has to be found.

3.2 Thermal Behavior

Power is generated by two sources and entirely dissipated as heat. Pump power and friction power. Pump power is the energy that forces the fluid through the bearing. Friction power is the energy necessary to move the carriage. Both are dissipated due to viscous shear losses in the bearing. The calculation of power assumes laminar flow in all parts of the bearing the bearing pockets, the bearing lands and the fluid supply lines. The area where turbulence is most likely to occur are the bearing pockets. Thus, the condition for laminar flow in the bearing pocket is a Reynolds number

$$Re = \frac{v h_p \rho}{\mu} \quad (3.52)$$

smaller than 2000. Turbulent flow, i.e. large Reynolds numbers, increases the friction in the fluid and the shear stress on the walls significantly and therefore leads to a significant increase in temperature. The equation stated are not valid for this case.

The pump power is calculated as the product of total fluid flow and supply pressure. With the fluid flow Q as derived earlier the total pump power becomes

$$P_p = Qp_s = \frac{p_s^2}{R} \quad (3.53)$$

The friction power which must be transmitted through the moving surface is the product of the friction force and the surface speed. The equation for the shear stress according to Newtons law of viscosity of two plates moving relative to each other at a distance h

$$\tau = \eta \frac{du}{dy} = \eta \frac{v}{h} \quad (3.54)$$

and the force required to shear a surface of area A

$$F = A\tau \quad (3.55)$$

lead to the equation for the friction power

$$P_f = F_f v = \mu v^2 \left(\frac{A_{land}}{h} + \frac{4A_{pocket}}{h_p} \right) \quad (3.56)$$

It should be noted that the pocket area contributes to a larger extent to the friction losses than the land areas. The factor four accounts for these addition losses considering recirculating flow in the pocket. The total power generated in hydrostatic bearings is the sum of the pump and the friction power

$$P_{total} = P_p + P_f \quad (3.57)$$

Another alternative form of this equation is

$$P_{total} = P_p (1 + K), \text{ with } K = P_f/P_p \quad (3.58)$$

where K is the power ratio also indicating the proportion of hydrostatic to hydrodynamic effects. Pure hydrostatic load support leads to $K=0$, what in fact means zero velocity between the parts. According to this characteristic K can be used as a measure for distinguishing hydrostatic bearing in 'low speed' bearings with $K < 1$ and 'high speed' bearings with $K > 1$.

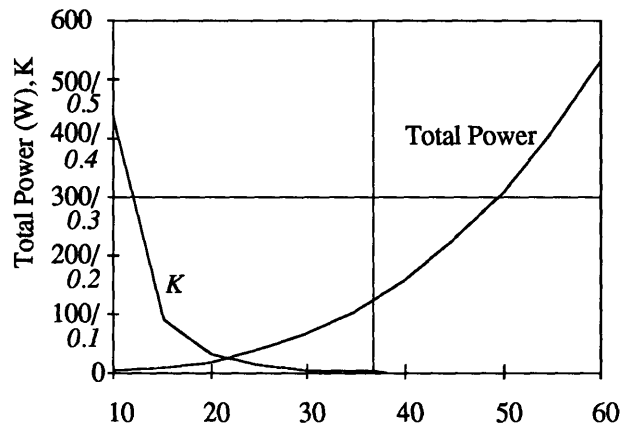


Figure 3.8: Total power and power factor K for changing nominal gap.

From Figure 3.8 shows the total power and the power ratio K for a linear hydrostatic bearing running with a velocity of 0.5 m/sec (30 m/min). A larger gap influences the total power significantly increasing the pump power exponentially. As the gap decreases the shear power gains relative to the pump power more importance, but due to low speeds never reaches a level dominating the total power. Since linear hydrostatic bearings seldom move faster than 0,5 m/sec they can generally be regarded as low speed bearings. For the bearing configuration simulated above, using water as fluid and a supply pressure of 10 atm, the total power at a 10 μ m gap is only 3.5 W.

The factor K indicates that the shear power never accounts for more than 50 % (i.e. at a 10 μ m gap $K=0.425$ and $P_f \approx 1.5W$) of the total power. This is due to the decreasing flow rates of the bearing. At laminar speeds using water with its low viscosity ($\mu=0.001$ Nsec/m²) decreases the power generated by an order of magnitude compared with normally used oil (ISO 10 oil with $\mu=0.01$ Nsec/m²). In addition, the water has twice the heat capacity of oil. In order to achieve the same magnitude of total power for oil bearings the gap has to be expanded reducing stiffness and load capacity significantly.

The temperature rise in the fluid from the entry of the bearing to the end of the bearing can be calculated assuming that the energy is convected from the bearing.

$$\Delta T = \frac{P_{total}}{Jc\rho Q} \quad (3.59)$$

Most machines require that minimum heat is introduced into the machine. Thus, it is necessary to minimize the power for a given load capacity. Minimizing the total power is achieved by minimizing the fluid flow and increasing the heat capacity of the fluid. Small bearing gaps produce small flow rates, since the resistance of the bearing is inversely proportional to the cube of the bearing gap and hence lowering power generated. However the friction power increases with smaller gaps and can produce an significant amount of heat at higher speeds. Low speed bearings don not suffer from this particular problem especially when using a low viscosity fluid.

3.3 Design of Flow Restrictors

As it was shown, hydrostatic bearings need a flow restrictor in order to support varying loads. There are four different types of bearings, distinguished by the kind of flow restrictor that regulates the inlet-flow into the bearing pocket. All provide the necessary pressure difference to support varying loads. However, the design of flow restrictors is critical, since it determines the overall performance of the bearing and the cost to a large extent. This thesis is concerned with the design of bearings using self-compensation, the other compensation methods are described only briefly.

3.3.1 Constant flow devices:

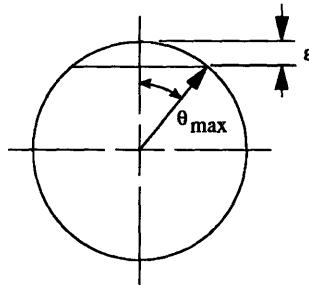
To provide constant flow to the bearing pockets, regardless of the bearing gap displacement is achieved by several methods. One uses one pump per bearing pad, but since this method is expensive more often a single pump and flow dividers are used to distribute the flow equally to the bearing pockets.

This methods provides the largest stiffness, but is expensive and due to the tendency of normally used oil to change the viscosity with changing temperature the undesired amounts of fluid flow can degrade the performance of the bearing or in the extreme the bearing is not able to support any load at all.

3.3.2 Laminar flow devices with fixed compensation:

There are several restrictor providing a fixed restrictor resistance regardless of the operating conditions, i.e. changing bearing gap. Most of them make use of the fluid resistance of small diameter passages. Flat edge pins, when pressed in a hole provide simple means of creating a resistance. As also do capillary tubes of small inner diameter. In order to achieve the desired resistances the diameter have to be on the order of 0.4 mm.

$$\Theta_{\max} = a \cos \left(1 - \frac{2\varepsilon}{d_p} \right)$$



$$R = \frac{192\mu l}{d_p^4 f(Q_{\max})}$$

Figure 3.9: Flat-edge-pin: Laminar flow devices with fixed compensation

There are several disadvantages associated with fixed compensated hydrostatic bearings. Load capacity and stiffness are half of self-compensating bearings and the flow in the restrictors tends to turn turbulent and therefore generates undesired heat and mechanical noise. The small diameter passages tend to clog and due to the sensitivity to manufacturing errors both compensation devices must be expensively hand-tuned during assembly in order to match the bearing pad resistance and to optimize performance.

3.3.3 Laminar flow devices with variable compensation

Laminar flow devices with variable compensation, as the type shown in Figure 3.10 include the use of diaphragms or valves to provide a flow inversely proportional to the pocket resistance. Thus, they create a larger differential pressure than created with the use

of fixed compensation devices. Even they achieve higher performance than fixed compensated bearings, they suffer from all other disadvantages described for fixed compensated bearings.

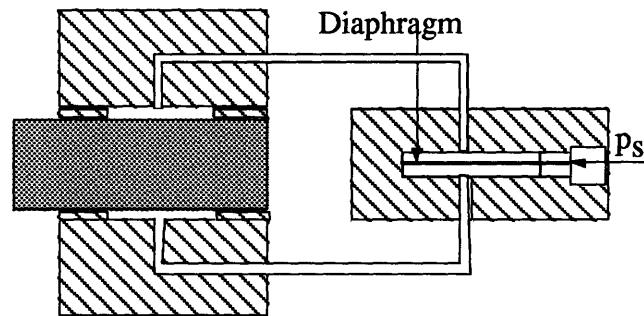


Figure 3.10: Variable compensation device (Diaphragm-Type)

3.3.4 Laminar flow devices with self-compensation:

Self-compensation, according to the principle of self-help [5], is based on the principle that high pressure fluid can be regulated through passages on the bearing surface. The restrictor resistance is achieved by the same means as the bearing pad resistance. The fluid then flows to the opposed bearing pocket. All self-compensated bearing designs follow this principle. There are a variety of self-compensated bearing designs, first developed during the 1940's. They all suffer from detrimental fluid flows, which decreases the performance. In addition due to the complex fluid pattern, they are not deterministic and their performance is difficult to predict. But these effects can be eliminated by proper design of the compensation devices. A new design, called Hydroguide™ is described in detail.

As shown in Figure 3.11 and 3.12 the fluid flows out of the pocket on the surface of the bearing, across restrictor lands, whose area is tuned to that of the opposed pocket's land. It then flows into the small collection pocket that is connected to a large bearing pocket on the opposite side of the bearing rail. The resistance of the compensator, and therefore the flow is now controlled by the change in bearing gap. The compensation device and the corresponding bearing pocket experience the same magnitude of displacement, but with different signs. When a positive load is applied the load bearing's gap decreases resulting in increasing flow resistance. The corresponding compensator gap increases, decreasing the flow resistance, and thus providing a larger flow to the bearing pad that is resisting the load.

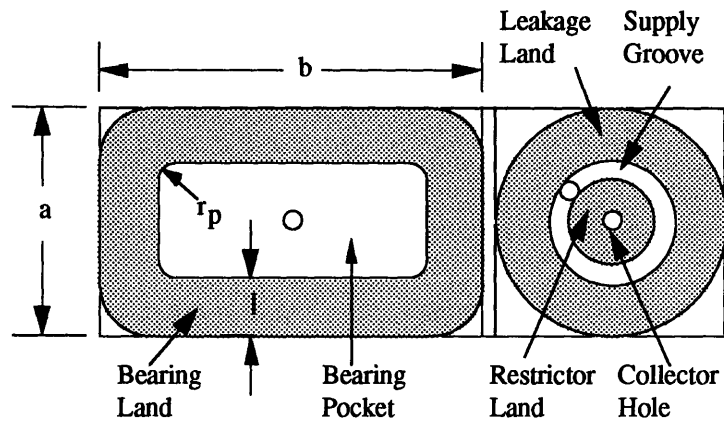


Figure 3.11: Bearing pad and restrictor pad geometry

A new design is proposed, called Hydroguide™. It overcomes the disadvantages generally associated with hydrostatic bearings. The Hydroguide™ has a compensator geometry leading to flow pattern accurately known in advance. The flow restrictor consist of round and linear lands with the least complex shape. The least complex shape, not incorporating linear lands is a complete annulus as shown in Figure 3.11. The flow pattern is constant and easy to analyze. The results of the analysis can be easily incorporated into spreadsheets accurately predicting the performance of different bearing configurations.

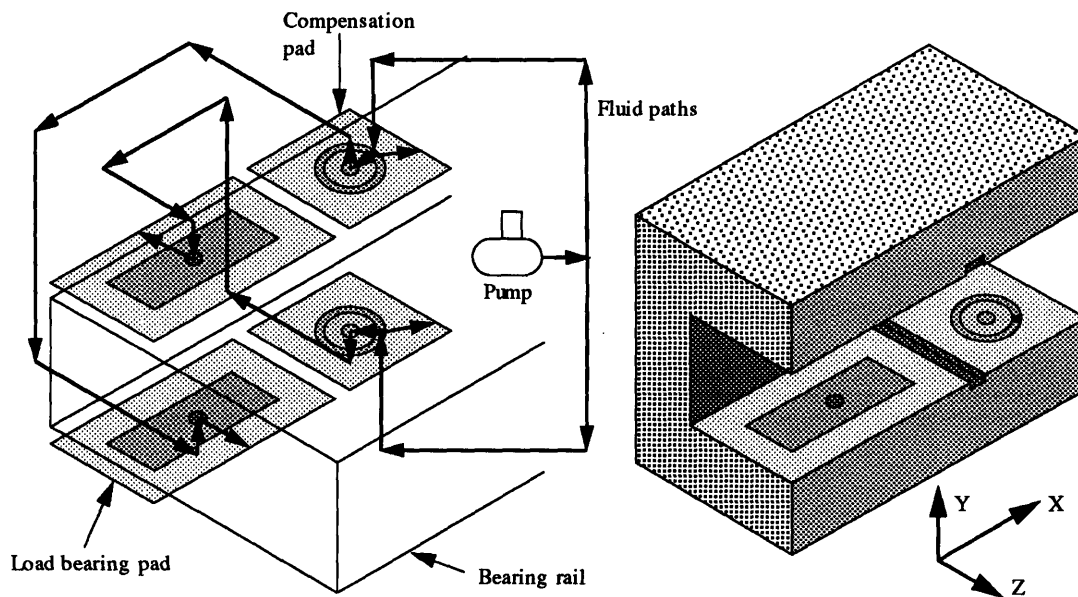


Figure 3.12: The principle of self-Compensation using Hydroguide™.

Since it has no small diameter passages (the smallest diameter hole is 3-5 mm) the bearing does not tend to clog. Even in case of contamination, small parts supplied with the fluid to the compensator will be ground away in the bearing gap through the moving carriage. Thus the bearing is entirely self-cleaning.

The effect of self-cleaning and the insensitivity to contamination allows the use of water as bearing fluid instead of normally used oil. Water has the inherent property to self-contaminate through biological effects and is not suitable for other bearing designs. It has a high heat capacity and excellent thermal conductivity. This reduces the heat generated by the bearing and results in a smaller temperature increase.

Due to the low viscosity of water the bearing gap can be as small as reasonable to manufacture. While oil hydrostatic bearings require nominal bearing gaps of 30-40 μm it can be decreased for water hydrostatic bearing to 10 μm . This increases load capacity and stiffness as well as damping. Due to the higher flow resistances the fluid flow decreases resulting in lower pump power.

Self-compensated bearing have no need for hand-tuning. Changes in gap, due to manufacturing errors influence the bearing and the compensator equally and the resistance bridge remains balanced.

The performance of this type of hydrostatic bearing in terms of load capacity/area and stiffness/area is higher than of all other bearings discussed. As it will be seen, its load capacity and stiffness are approximately twice of fixed compensated bearings.

Load capacity

Applying the analysis described in chapter 3.1 to the restrictor resistances the load capacity is determined as the product of the differential pocket pressure times the effective area.

$$F = A_{eff} P_s \left(\frac{\frac{1}{(h-\delta)^3}}{\frac{\gamma}{(h+\delta)^3} + \frac{1}{(h-\delta)^3}} - \frac{\frac{1}{(h+\delta)^3}}{\frac{\gamma}{(h-\delta)^3} + \frac{1}{(h+\delta)^3}} \right)$$

The load capacity changes with changing resistance ratio γ , decreasing slightly with increasing γ . Figure 3.13 shows a typical load capacity curve of a self-compensated bearing as function of displacement δ ($\gamma=1$ to $\gamma=10$). It has an effective bearing pad area

of 6140 mm², a nominal bearing gap of 15 μm, a supply pressure of 10 atm and uses water as bearing fluid ($\mu=0.001$ Nsec./m²).

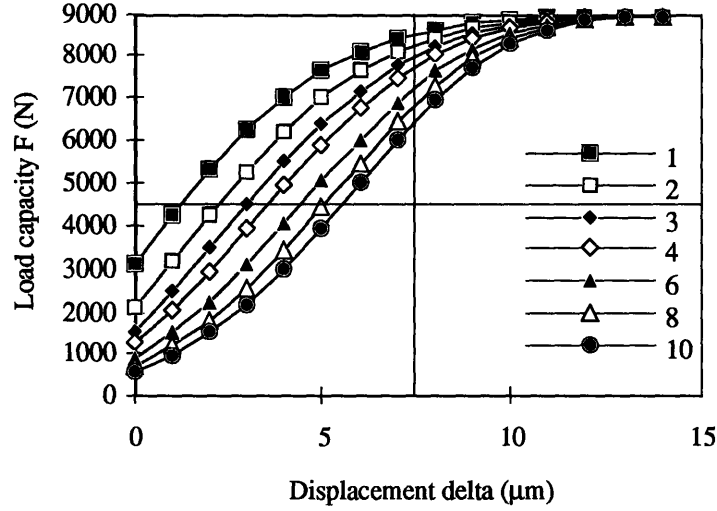


Figure 3.13: Load capacity of a self-compensated hydrostatic bearing.

Stiffness

The partial derivative of the load capacity with respect to the displacement delta is the stiffness and yields:

$$K = F \frac{\partial}{\partial \delta}$$

$$K = 3A_{eff} p_s \left[\frac{\frac{\gamma}{(h-\delta)^4} - \frac{1}{(h+\delta)^4}}{(h+\delta)^3 \left(\frac{\gamma}{(h-\delta)^3} + \frac{1}{(h-\delta)^3} \right)^2} + \frac{1}{(h+\delta)^4 \left(\frac{\gamma}{(h-\delta)^3} + \frac{1}{(h-\delta)^3} \right)} \right. \\ \left. + \frac{-\frac{1}{(h-\delta)^4} + \frac{\gamma}{(h+\delta)^4}}{(h+\delta)^3 \left(\frac{1}{(h-\delta)^3} + \frac{\gamma}{(h+\delta)^3} \right)^2} + \frac{1}{(h-\delta)^4 \left(\frac{1}{(h-\delta)^3} + \frac{\gamma}{(h+\delta)^3} \right)} \right]$$

As for the load-capacity the stiffness change with changing γ . The effect is seen in Figure 3.14 for $\gamma=1$ to $\gamma=10$. As the resistance ratio increases the stiffness gets more uniform for displacements δ . But for a displacement of 25 % of the nominal bearing gap the stiffness decreases, compared with the maximum value for $\gamma=1$.

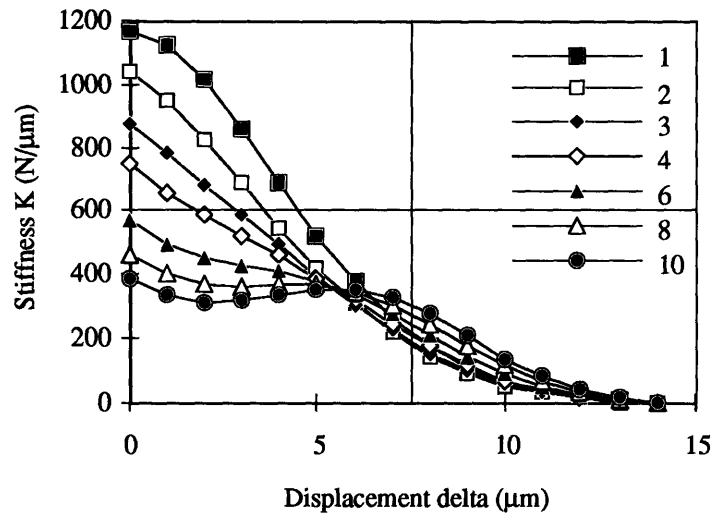


Figure 3.14: Stiffness of a self-compensated hydrostatic bearing.

A lower stiffness may also be desirable to achieve a balanced design, preventing the bearing from being too stiff compared with the machine structure. With decreasing stiffness the damping capability of the bearing increases providing better dissipation of energy introduced by other machine elements.

4. Comparison of Self- and Fixed-Compensated Hydrostatic Bearings

Using the spreadsheets written for both types of bearings a comparison of hydrostatic bearings with fixed and hydrostatic bearings with self-compensation can be easily done by parameter studies. The two bearings analyzed are similar, distinguished only by the kind of compensation. The supply pressure is 10 atm, the bearing gap is 15 μm and the bearing fluid used is water. Note that a bearing gap of 15 μm and the use of water is desirable as described above but can only be realized using the principle of self-compensation. In order to analyze the differences between the compensation methods this is neglected.

The bearing parameters are:

<i>supply pressure</i>	<i>ps (atm, Pa= N/m²)</i>	10	<i>1,013,250</i>
	<i>ps (psi)</i>	147	
<i>dynamic viscosity</i>	<i>μ [μ] (Nsec/m²)</i>	0.001	
<i>density ρ</i>	<i>rho (kg/m³)</i>	997	
<i>pocket depth</i>	<i>hp (μm, m)</i>	300	<i>0.000300</i>
<i>nominal bearing gap</i>	<i>h (μm, m)</i>	15	<i>0.000015</i>
<i>restrictor/bearing pad ratio</i>		1	

4.1 Load Capacity and Stiffness

Load capacity and stiffness of self-compensated hydrostatic bearings are approximately twice the value as for hydrostatic bearings with fixed compensation for a bearing/restrictor resistance ratio of 1. Figure 4.1/4.2 and Figure 4.3/4.4 show the load capacity and stiffness of this bearing configuration as a function of displacement δ . In order to provide a stiffness that has constant value over the range of displacement typically allowed in bearing applications, the bearing/restrictor resistance ratio should be about 3 to 4 with stiffness values still greater than for fixed compensated bearings.

It should be noted that increasing load capacity and stiffness of fixed compensated bearings to the level of self-compensated bearings by means of higher supply pressure results in higher pump power and therefore is not desirable.

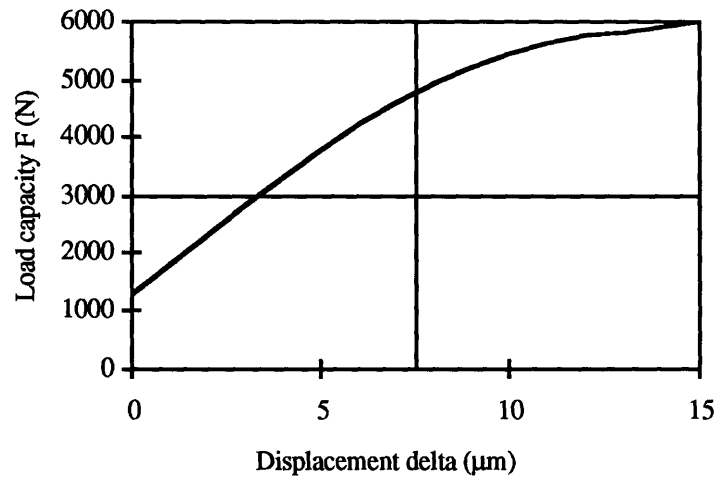


Figure 4.1: Load capacity of a fixed-compensated hydrostatic bearing.

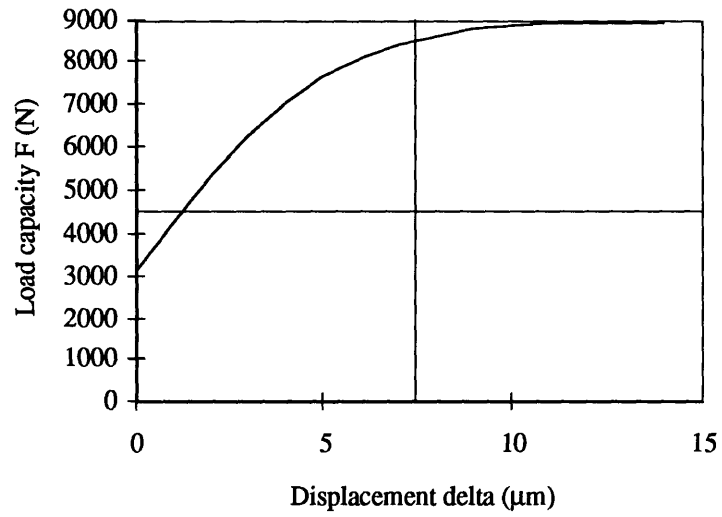


Figure 4.2: Load capacity of a self-compensated hydrostatic bearing (Hydroguide™).

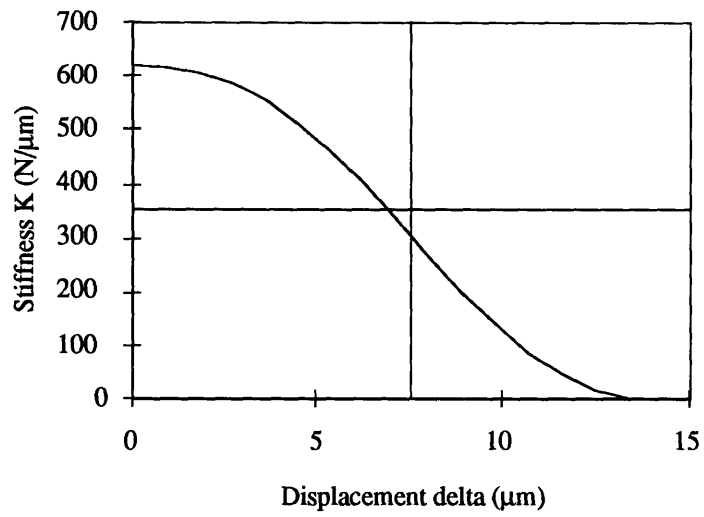


Figure 4.3: Stiffness of a fixed-compensated hydrostatic bearing.

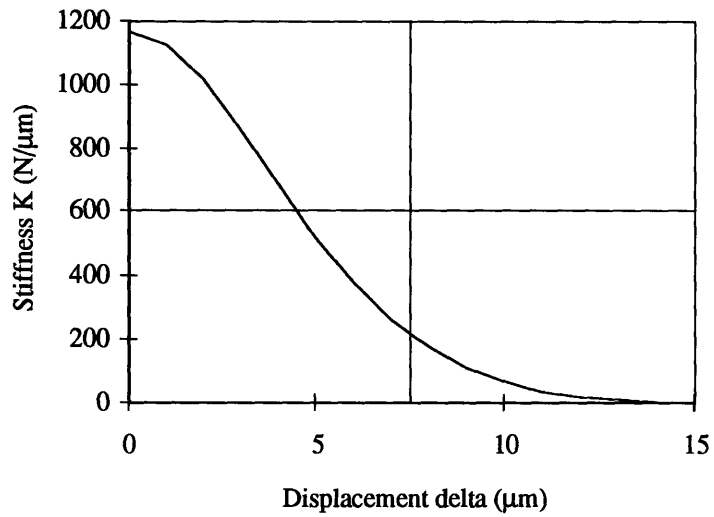


Figure 4.4: Stiffness of a self-compensated hydrostatic bearing (Hydroguide™).

4.2 Manufacturing Error

The performance of hydrostatic bearings is to a large extent influenced by the nominal bearing gap. Therefore, with variations in bearing gap due to manufacturing errors the bearing is subjected to significant variations in performance. The actual bearing gap considers the error due to manufacturing errors and is described by the following equation:

$$h_{actual} = h_{ideal} + error$$

The actual stiffness of the bearing is determined by implementing the actual bearing gap into the stiffness equation derived. The %-variation in stiffness is

$$\% \text{-variation in stiffness} = 100 \frac{(K_{actual} - K_{ideal})}{K_{ideal}}$$

with the ideal stiffness being the stiffness without manufacturing errors. Figure 4.5 and 4.6 show the %-variation in stiffness for a self- and a fixed compensated bearing as a function of manufacturing error for different nominal bearing gaps.

As seen in Figure 4.5 and 4.6 the self-compensated bearing shows a much smaller variation in stiffness for various manufacturing errors than the fixed compensated bearing. The latter is subjected to a significant loss in performance when the bearing gap varies due to manufacturing errors. Furthermore the restrictor resistance does not experience the same error and the resistance bridge becomes unbalanced. Therefore it requires careful hand-tuning of the flow restrictors to optimize performance. Self-compensated bearings are less sensitive to manufacturing errors and since bearing and restrictor pad experience exactly the same manufacturing error the resistance bridge stays balanced under all conditions and no hand-tuning is required.

This is especially important for decreasing nominal bearing gap, since smaller bearing gaps increase the performance and are in most applications preferred. The smaller the bearing gap becomes the less sensitive gets the self-compensated bearing while the %-variation in stiffness of fixed compensated increases.

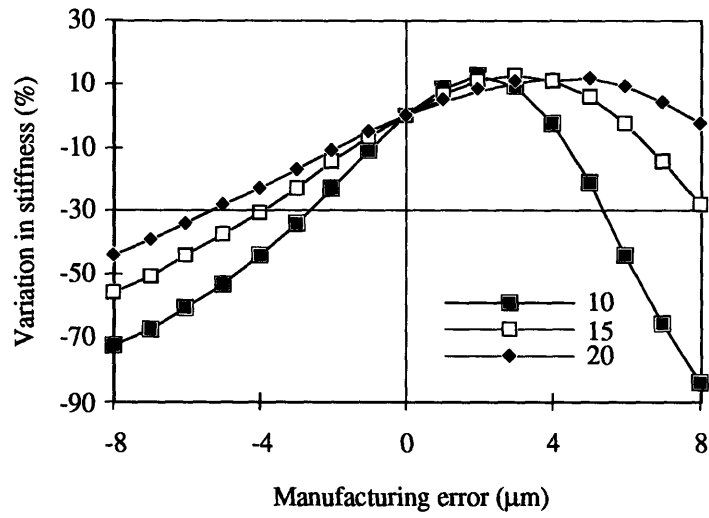


Figure 4.5: Manufacturing error of a fixed-compensated hydrostatic bearing.

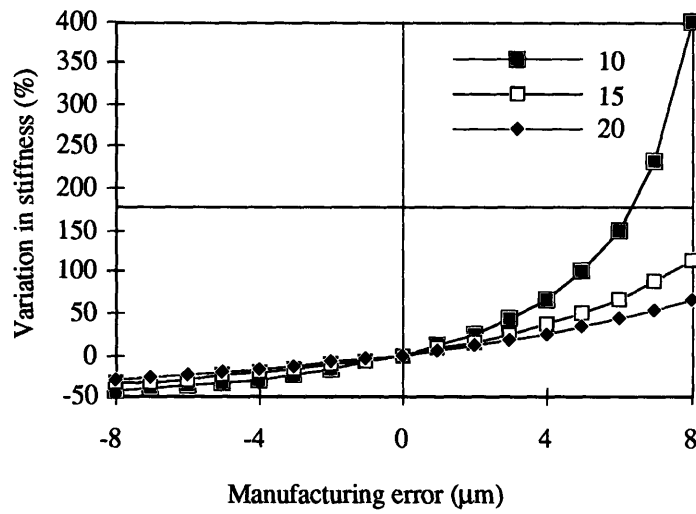


Figure 4.6: Manufacturing error of a self-compensated hydrostatic bearing.

4.3 System Design

When designing hydrostatic linear motion bearings, requirements are often given in terms of stiffness and load capacity at a maximum displacement, maximum carriage velocity and available space for implementation. The bearing parameters have to be carefully chosen in order to achieve a good hydrostatic bearing complying with the specifications. Fixed and self-compensated bearings are discussed.

Supply Pressure

The supply pressure is determined by the desired load capacity and stiffness. Assuming that the bearing geometry is chosen the supply pressure can be varied according to the performance specifications. It is important to note the limits in supply pressure. First, higher supply pressure requires more pump power, resulting in an increase in temperature of the fluid. Furthermore, the higher the supply pressure the higher the pressure fluctuations introduced into the system. This is especially true for fixed compensated bearings with their low stiffness and load capacity values compared with self-compensated bearings. The supply pressure has to be significantly higher in this type of bearing.

Bearing Fluid

Normally used oil has the desired lubrication properties and is long term stable. It is used for fixed compensated bearings to make them work reliably. But oil has a high viscosity, limiting the reduction of the bearing gap and is environmentally unfriendly. Water, used in self-compensated bearings has a lower viscosity than oil and is environmentally friendly. In addition it has a higher heat capacity and excellent thermal conductivity. Lower viscosity reduces the necessary pump power and prevents the fluid film from building up hydrodynamic wedges at higher speeds. If water is used as a bearing fluid it should have biocidal and fungicidal additives. In addition, a water solvable lubricant may be added for increased pump life. Even it is theoretically possible to use water as fluid in fixed-compensated bearings, due to the compensation devices lack of self-cleaning this configuration is not used in practice.

Bearing Pad Geometry

The land width of linear hydrostatic bearings is typically 25% of the pad width but may have to be decreased for high speed applications in order to minimize the viscous shear and to prevent the bearing from running dry. The lands should always be large enough to support the weight of the carriage when the supply pressure is turned off. The pocket should be at least 10-20 times the nominal bearing gap for linear applications. When additional squeeze film land in the pocket are added, it must be assured that the bearing still can be lifted from rest and the water is evenly distributed to the bearing lands.

Nominal Bearing Gap

The bearing gap in linear applications should be as small as possible, increasing load capacity, stiffness and damping and minimizing the required pump power. Smaller bearing gaps also increase the viscous shear generated in the bearing gap. However, linear application do not suffer from excessive heat generated through this effect due to relatively low speeds (30m/sec). The smallest nominal gap reasonable to manufacture is about 10 μm . Since fixed compensated bearings usually use oil as fluid the gap has to be larger than for self-compensated bearings. This results in decreased bearing performance.

Design for High Speed

For high speed applications for both bearing designs the same considerations apply. Careful calculations of the lowest fluid velocity in the bearing system have to be carried out in order to ensure that the fluid velocity is always larger than the carriage velocity. If the fluid velocity is too small, air is dragged into the bearing reducing the performance significantly. If necessary the fluid velocity can be increase by choosing a larger bearing gap to the detriment of load capacity and stiffness. The maximum speed of the carriage supported by a bearing with $\gamma=1$ and the smallest pocket pressure p is

$$v_{\max} = \frac{ph^2}{12l\mu}$$

In order to keep the fluid velocity high while a load is applied the bearing should experience zero displacement under these conditions maximizing the smallest bearing gap. This is achieved by unequally sized bearing pad. In addition, often the rail geometry requires unequally sized bearings, in order to utilize the entire width of the bearing rails and stiffness and load capacity requirements apply only in one direction. As a consequence the preload bearing pad can be of smaller dimension. In contrast to equally sized bearing pads, bearings having unequally sized bearing pads with the load bearing pad being larger than the preload bearing pad experience a displacement δ opposite to the regular direction of loads when no load is applied. Since the smallest bearing gap determines the maximum allowable carriage velocity it is desirable to operate the system under load at zero displacement.

The negative displacement at zero load is due to the fact that the force of the load bearing pad is larger than the force of the preload bearing pad since $A_{Load} > A_{Preload}$ and $p_{Load} = p_{Preload}$.

$$F_{Load} = A_{Load} \cdot p_{Load} > F_{Preload} = A_{Preload} \cdot p_{Preload}$$

Thus, the bearing will be lifted, decreasing the preload bearing pad's flow resistance and pocket pressure and increasing the load bearing pad's flow resistance and pocket pressure until force equilibrium $A_{Load} \cdot p_{Load} = A_{Preload} \cdot p_{Preload}$ is reached at a displacement. The average workpiece load, the minimum and the maximum load should be considered, reaching zero displacement for the load applied to the bearing.

Design for Low Power Generation

The total power of the hydrostatic system consist of the pump power and the friction power. Since the friction power is insignificant for linear applications the pump power has to be minimized. In order to reduce the required pump power the fluid flow must be minimized. This is achieved using small nominal bearing gaps providing larger flow resistances. Since load capacity and stiffness increase with decreasing gap the pump power can be further reduced to match the specifications.

Design for Manufacturability, Assembly and Maintenance

Hydrostatic bearing pad geometries are easy to manufacture with a high degree of accuracy. Bearing gaps of 10-20 μm , desired for high performance, can be manufactured with reasonable effort. In addition, hydrostatic bearing pads are self-cleaning and can not be contaminated with dirt. This applies only for bearing pads. Restrictors are discussed separately

Fixed compensated bearings use flat-edge pins or capillary tube in order to provide the necessary restrictor resistance. Variation in the bearing gap due to manufacturing errors lead to the necessity of hand-tuning the resistance of the restrictor to the resistance of the bearing for maximum performance. This process, based on experience is time consuming and costly considering at least twelve bearing pads are used in machine tool application in order to restrict five degrees of freedom.

Fixed resistance restrictors have very small diameter passages (ca. 0.4mm) that tend to clog during operation. Last chance filter screens have to be used to prevent the bearing from failing. Since capillary tubes and flat-edge pins are not self-cleaning they have to be disassembled from the machine for maintenance on a regular basis. Adjusting and maintaining fixed-compensated hydrostatic bearings is time consuming and cost intensive.

Self-compensated bearings are less sensitive to manufacture and require no hand-tuning since the resistance bridge remains balanced even with manufacturing errors introduced. The compensation device is self-cleaning and there are no smaller passages than 3-5 mm in diameter.

5 Case Study 1: Low Pressure Bearing

To illustrate the design of linear hydrostatic bearings using the Hydroguide™ a first prototype bearing was designed. Its intention was to proof the feasibility of the working principle and verify the theory developed for the Hydroguide™. A large scale model was build as shown in Appendix B. This bearing was designed for small supply pressure of only 20 psi. Due to its simplicity the manufacturing effort was kept to a minimum.

The bearings are designed using a spreadsheet developed shown in appendix A. All important performance measures are predicted according to the formulas derived earlier. The spreadsheet guided the design of the bearing pads and its output was compared with the experimental data collected.

5.1 Design Considerations

The bearing uses bearing blocks incorporating each a set of opposed hydrostatic bearing pads and their restrictors shown in Appendix B. These bearing blocks, four to support the carriage vertically and two to support the carriage horizontally, are connected to the carriage. In addition to incorporating the bearing geometry, they distribute the fluid from the supply line through fluid connections by means of holes drilled. The carriage and the bearing blocks ride on the base and rails attached to the base. The principle is illustrated in Figure 5.1. With a base of 1200 mm and a carriage 600 mm long a 600 mm range of travel was realized.

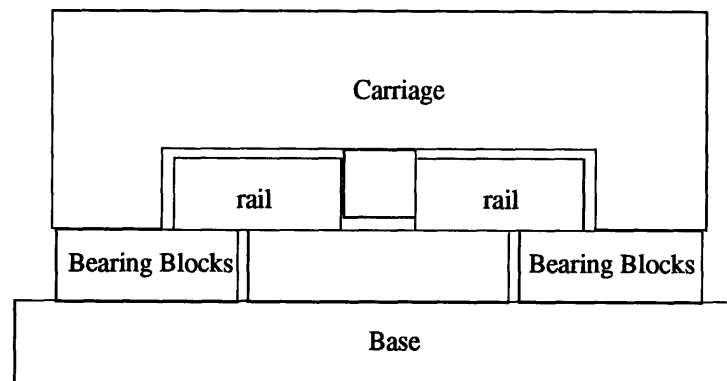


Figure. 5.1: Schematic of the hydrostatic bearing design using bearing blocks..

All structural parts, the base, the carriage, the rails and the spacer between the rails and the base as supporting and guiding elements were made from granite. Granite has a low coefficient of thermal expansion, is easy to manufacture with a high degree of accuracy and has good damping capabilities. On the other hand it has a low coefficient of conductivity and tends to absorb water. While the former was of smaller importance for this test bearing, the latter was solved by treating all granite surfaces with a dissolved acrylic. Since it provided the high degree of accuracy for low cost granite was chosen as structural material.



Figure. 5.2: Low pressure hydrostatic test bearing.

The bearing blocks were made from stainless steel with a replicated layer of epoxy on each side containing the bearing geometry. A drawing of a vertical bearing block is shown in Appendix B. The stainless steel chosen is corrosion resistant and reasonably to manufacture. Both important criteria since water is used and long holes had to be drilled connecting the bearing and restrictor pads. The replication epoxy eases the manufacturing process and provides excellent emergency running properties. The disadvantage of absorbing water over time and due to the swelling of the material decreasing the bearing gap was solve by treating it with a dissolved acrylic as it was done with the granite.

This bearing was restricted to low supply pressure because as a preloaded bearing systems the bearing blocks induced deformations into the bearings granite structure of

relatively low stiffness. Due to the use of unequally sized bearings in an opposed configuration as in case of this design the bearing blocks create a moment on the bearing blocks as shown in Figure 5.3. The moment not only tilts the bearing blocks with respect to the base, but also bends the low stiffness granite carriage. For this system the difference in gap between the two sides of the load bearing region was $1.1 \mu\text{m}/\text{atm}$. A changing bearing gap results in decreasing performance especially since the change in bearing gap is not sensed by the compensator. Therefore the system was restricted to 20 psi supply pressure, so the deformation was kept at about 10 % of the nominal bearing gap of $15 \mu\text{m}$.

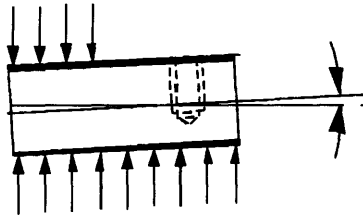


Figure. 5.3: Bending moment on bearing blocks

5.2 Manufacturing

The bearing was designed to minimize cost and manufacturing and assembly effort. The manufacturing effort was reduced by using the smallest number of parts possible with the smallest number of precision interfaces necessary. The spaces containing the bearing blocks had to guarantee a consistent nominal bearing gap for both bearing pads of combined $30 \mu\text{m}$. To assure the required straightness only nine surfaces had to be precision ground. All structural parts are connected by bolts, carefully tightened during assembly. The parallelism of the rail with respect to the horizontal bearing block could be achieved by using precision gauge blocks on each end aligning the rails.

Using the method of replication using special epoxy, e.g. Moglice™, the bearing geometry was brought onto the bearing blocks. The final accuracy, fitting the blocks to the dimension of the structure, was guaranteed by carefully lapping them to the final dimension. While holding the horizontal bearings in place parallel to the rail using shim stock the bearing blocks were screwed to the carriage.

5.3 Bearing Design

The design of hydrostatic bearings is restricted to a large extent by the geometry of the structure. Since for this test bearing no direct performance requirement existed, but that it had to meet the finally predicted ones the load bearing pad size and the preload bearing pad size was chosen according to the structure geometry as shown below.

<i>supply pressure</i>	<i>ps (atm, Pa= N/m²)</i>	1.3606	137,863
	<i>ps (psi)</i>	20	
<i>dynamic viscosity</i>	<i>μ [mu] (Nsec/m²)</i>	Water	0.001
<i>pocket depth</i>	<i>hp (μm, m)</i>	300	0.0003
<i>nominal bearing gap</i>	<i>h (μm, m)</i>	15	0.000015
load bearing pad:			
<i>bearing width</i>	<i>au (mm, m)</i>	110	0.11
<i>bearing length</i>	<i>bu (mm, m)</i>	110	0.11
<i>land width</i>	<i>lu (mm, m)</i>	15	0.015
preload bearing pad:			
<i>bearing width</i>	<i>al (mm, m)</i>	45	0.045
<i>bearing length</i>	<i>bl (mm, m)</i>	90	0.09
<i>land width</i>	<i>ll (mm, m)</i>	10	0.01

Figure 5.4 and 5.5 show the load capacity and stiffness of the system as a function of displacement as calculated by the spreadsheet. The carriage has a approximate weight of 80 kg resulting in a force of 780 N on the bearings. At zero displacement the carriage has a load capacity of 771 N and therefore under zero external load the bearing will be positioned at zero displacement.

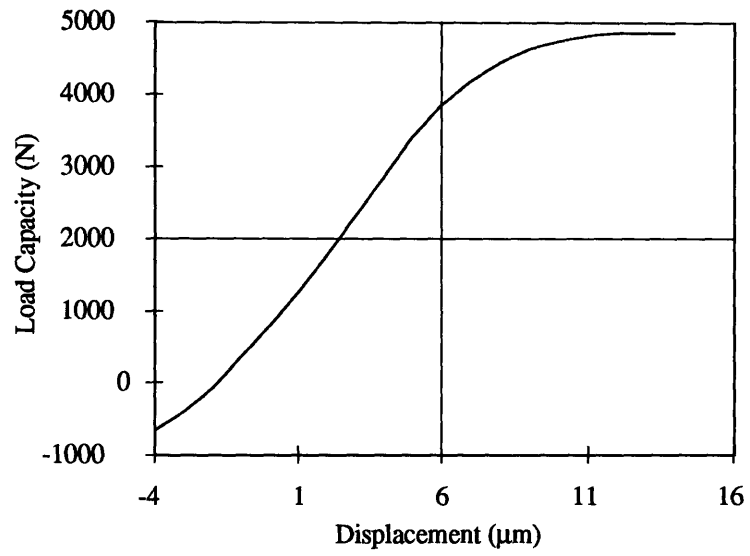


Figure. 5.4: Load capacity of the low pressure test bearing

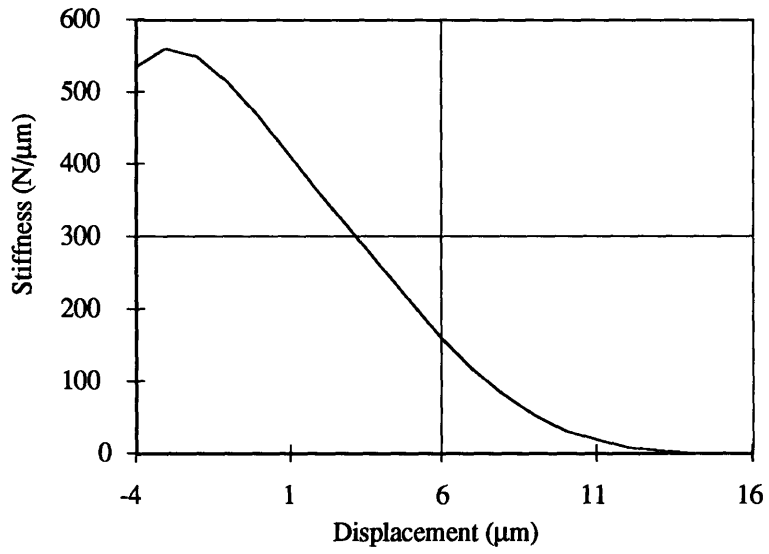


Figure. 5.5: Stiffness of the low pressure test bearing

5.4 Measurements

For the measurements a set-up was build consisting of the fluid supply system, an vibration isolated granite table to sustain the bearing and hard and software interfaces were established for the data acquisition. For the dynamic measurements a HP dynamic signal analyzer was used collecting impulse reposes of the carriage. Stiffness data were measured by using a capacitance ADE probe measuring the displacement of the carriage with respect to the base under static load. An OMEGA pressure transducer was used to determine the pocket pressure. A ZYGO AXIOM 2/20 laser interferometer measured linear displacement and straightness of the bearing. A beam was set up parallel and rectangular to the carriage and split to take measurements of the X and Z position of the carriage. Vertical motion was measured using a double path differential plane mirror interferometer (DPMI) on the carriage and a straightedge mounted on a bridge fixed with respect to the bearing. The straightedge functioned as a nearly perfect reference surface with a flatness of $\lambda/12$ over 18''.

5.3.1 Straightness

After the optics were carefully aligned the remaining noise level of the laser measurement system was measured with the carriage at rest. The measurement represents the noise of the laser measurement system due to alignment and environmental errors. The output of $0.025 \mu\text{m}$ is shown in Figure 5.6. The influence of the 20 psi supply pressure, taken from building water supply, is shown in Figure 5.6. With pressure supplied to the bearing pockets but with the carriage at rest the error motion was measured to be $0.03 \mu\text{m}$. It should be noted that at a higher supply pressure the pumps used introduces high levels of pressure fluctuations that result in corresponding error motions.

The straightness of the carriage depends on the shape of the base, the noise introduced by the fluid supply system and the tendency to build up hydrodynamic wedges during faster speeds. The supply pressure was only 20 psi and therefore the noise level due to pressure fluctuations introduced into the bearing so small, that they did not result in significant error motions as seen in Figure 5.7. Since hydrostatic bearings have very low friction, especially no static friction at all, the carriage could be pulled along the rail by gravity only. Therefore a smooth motion was realized without introducing detrimental forces at a speed preventing hydrodynamic wedges.

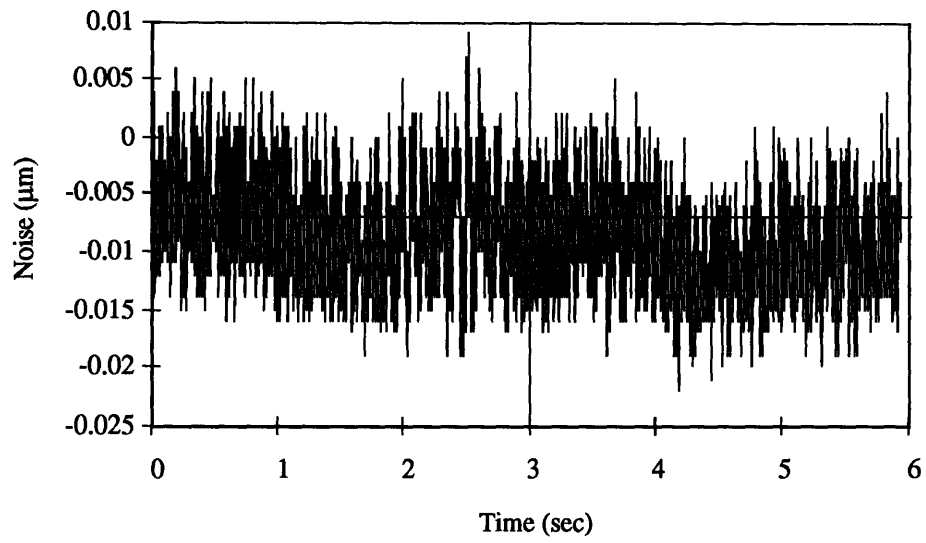


Figure. 5.6: Noise floor of the laser measurement system.

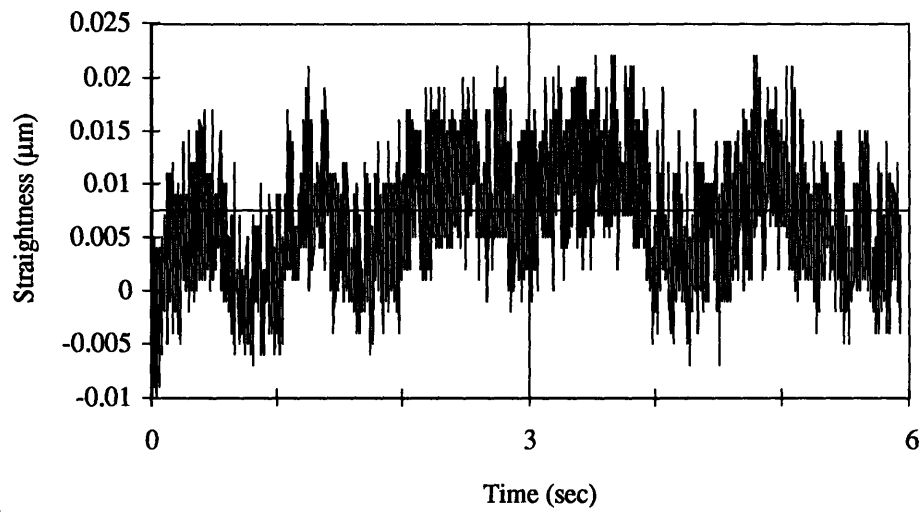


Figure 5.7: Error motion of the carriage with 20 psi supply y pressure .

The original distance of travel of 600 mm was reduced to 250 mm because parts of the optics were installed on the base of the bearing to decrease inaccuracies of the measurements due to motions of the base. Straightness data were taken over a distance of 235 mm and the trend removed using a linear trend removal algorithm. The overall straightness of the carriage, over a distance of 235 mm, is 1.6 μm as shown in Figure 5.8. This error motion is due to the first order straightness error of the bearings granite base. Figure 5.9 shows the spectral components of the straightness error. There are no significant peaks indicating that the bow is the only source of error. The assumption that the bolt pattern (10 mm bolt spacing) of the rails influences the straightness in this case proved not to be true.

Analyzing the same straightness data over a distance of 100 mm the straightness error reduces to 0.4 μm (Figure 5.10). Again, the conclusion is that this error is a result of the bearing base bow. The higher frequency error of the straightness measurement as shown in Figure 5.11. is 0.03 μm . This is the error of the measurement system as a comparison with Figure 5.7 of the measurement noise level shows. The straightness of hydrostatic bearings is insensitive to surface errors that are a fraction of the nominal gap height, due to the averaging effect of the large fluid film areas.

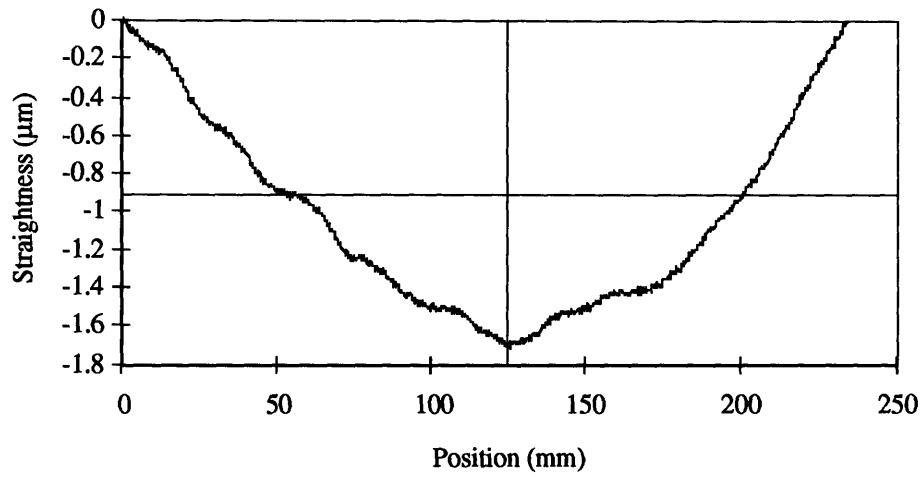


Figure. 5.8: Straightness (250mm) plot of granite bearing.

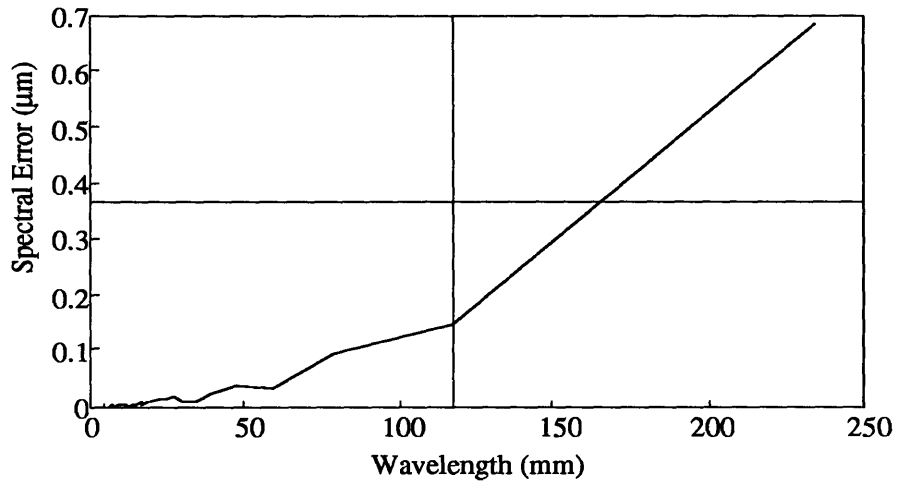


Figure. 5.9: The spectral components of the carriage's straightness error.

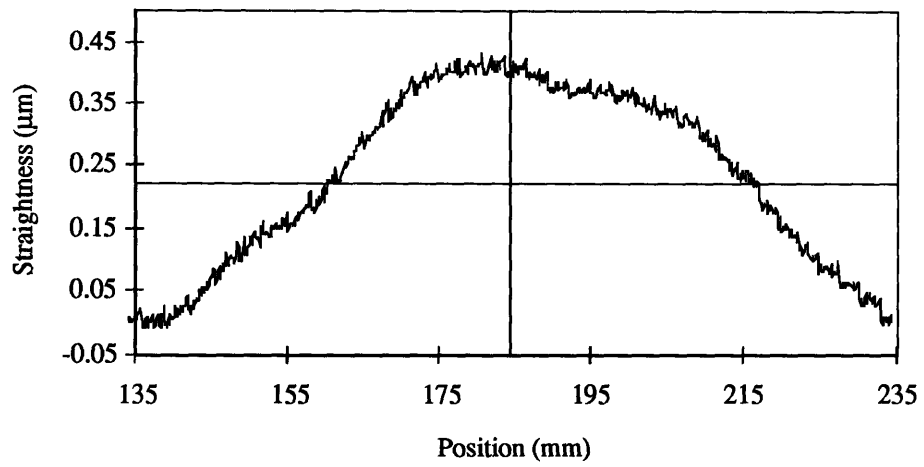


Figure. 5.10: Straightness (100 mm) plot of granite bearing.

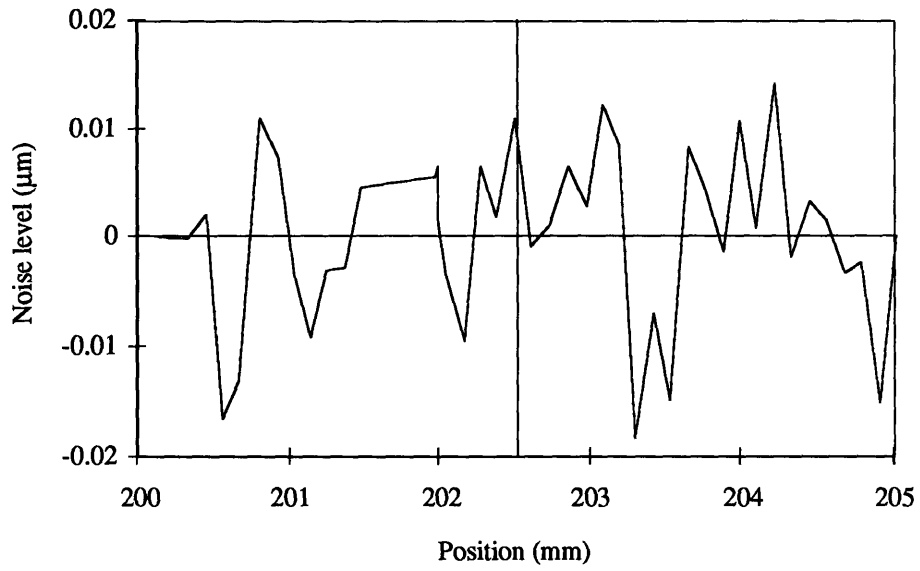


Figure 5.11: Noise level during straightness measurement.

5.3.2 Stiffness and Dynamic Response

Load capacity and stiffness for the bearing are determined analytically and shown in Appendix A. The experimental verification of these results was determined measuring the displacement and pocket pressure under static load. The former by loading the carriage with deadweights and measuring the displacement of the carriage with respect to the bearing base. The value was taken after the carriage settled from the applied load. The latter with a pressure transducer.

A capacitance probe with a nominal resolution of 5 nm measured the displacement of the carriage. As shown in Figure 5.12, the results reveal that from zero to maximum load the stiffness value is approximately linear, and about equal to $270 \text{ N}/\mu\text{m}$. The reason for the linear behavior, when a nonlinear behavior is expected, is due to the tilted bearing pad caused by the deformation of the bearing under pressure.

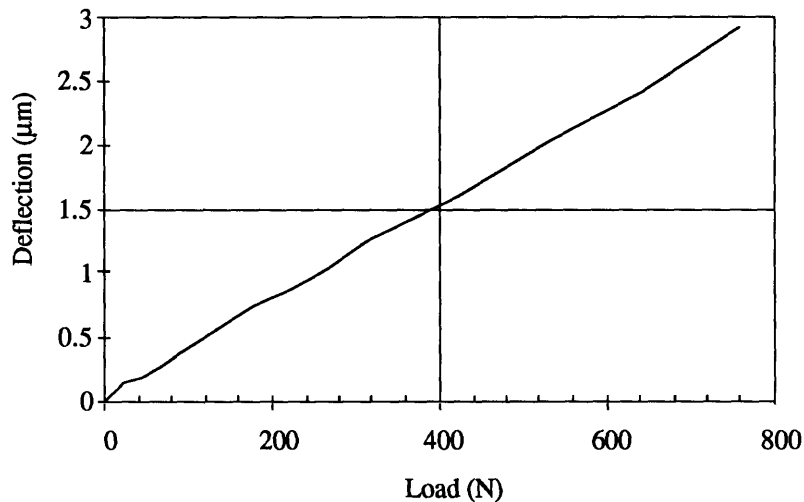


Figure 5.12: Bearing pocket pressure as a function of supply pressure.

The pressure measurement verify the effect of hydrostatic pressure induced deformations on bearing pocket pressure and therefore the stiffness. A supply pressure of 20 psi creates a bearing pocket pressure of 4 psi, which is consistent with the analytical value predicted by the calculation. At higher supply pressures, deformations cause a large increase in gap that is not sensed by the compensator. In the case of this bearing the difference in bearing

gap between the two sides of the load bearing pad was $1.1 \mu\text{m/atm}$. As a result, the pocket pressure drops and the performance decreases.

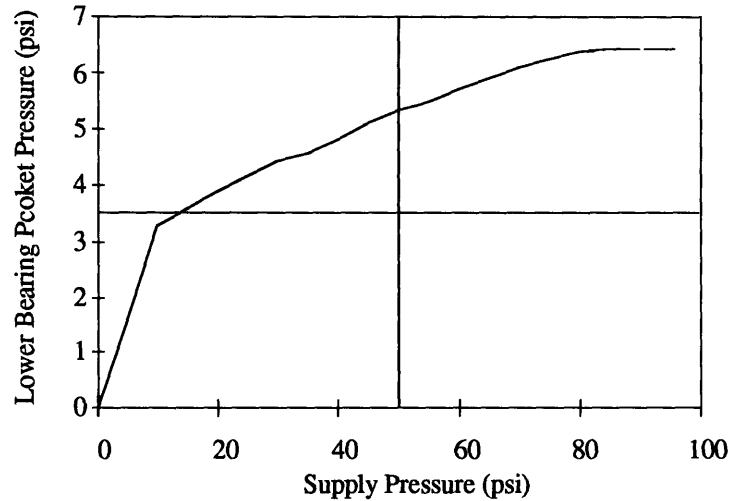


Figure 5.13: Bearing pocket pressure as a function of supply pressure.

In order to determine the dynamic stiffness of the system an impulse was applied to the carriage and the response measured with an accelerometer while collecting the data with a HP Signal Analyzer. Two different measurements were performed. The first measurement with of the system with no supply pressure and the carriage at rest. The second with the supply pressure turned on. Figure 5.14 shows the results two measurements.

The data taken include not only information about the motion of the carriage with respect to the bearing base, but about the entire system consisting of the bearing and the granite table on its air isolating system. Both curves combined indicate that all modes found are due to the motions of the granite base and table. Thus the carriage system motions are relative to these modes. Because the magnitude of the relative moving parts depends upon the stiffness and damping characteristics of the bearing system, it can be concluded that the system has a very high dynamic stiffness. The carriage/hydrostatic system itself does not show a separate mode because of the high degree of squeeze film damping.

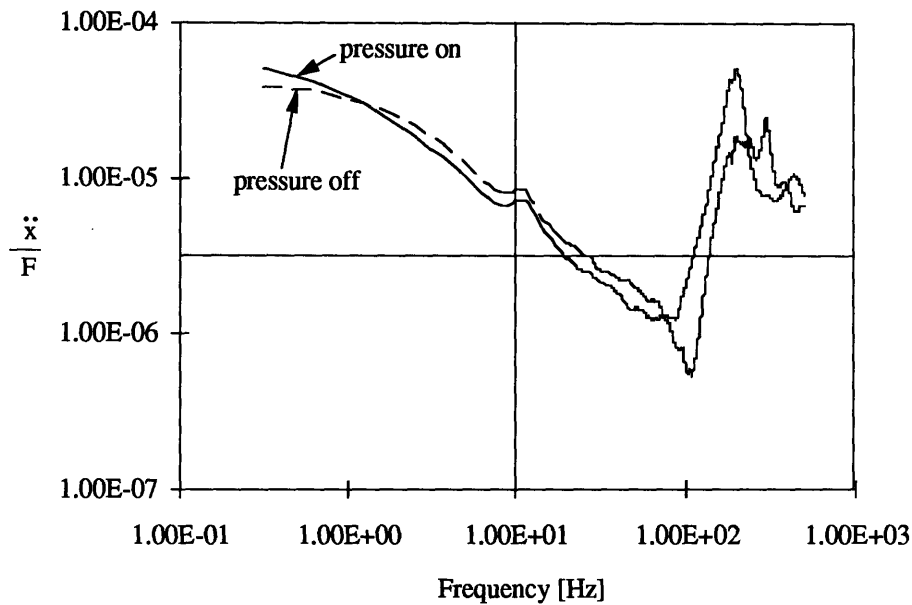


Figure 5.14: Dynamic response of the carriage with supply pressure on and off

Conclusions

As the first large scale bearing using the Hydroguide™, a self-compensated hydrostatic bearing, the test bearing was build to show the implementation of the principle and to proof the theory developed. It was designed as a inexpensive, easy to manufacture low pressure bearing. The theory was implemented into a spreadsheet guiding the design of the bearing and evolved for the use of design engineers not familiar in detail with this kind of bearing. Parameter studies can be performed to achieve a design complying with the requirements. This was possible since the Hydroguide™ is entirely deterministic.

The test bearing showed excellent straightness of 0.4 μm over a range of 100 mm and 1.6 μm over a range of 235 mm. There is no high frequency straightness error associated with this bearing. The measurement results comply with the spreadsheet data and therefore verify the theory. But the pressure in unequally sized bearing configurations induce deformations. Thus, the bearing gap changes not anticipated by the spreadsheet. The bearing has extreme damping capabilities due to its small bearing gaps. The overall dynamic response of the bearing as well as the performance of the bearing in terms of stiffness and load capacity is not only depended on the parameters described in the theory, but to a large extend by its structural components.

The bearing was run over one year on Cambridge tap water, a major part of that time without changing the water from the fluid circuit, without failure. It is self-cleaning, and robust against contamination.

6. Case Study 2: High Pressure Bearing

In order to achieve high load capacities and stiffness hydrostatic bearings designs must be able of high supply pressures. For these applications a bearing was designed for up to 300 psi supply pressure and accordingly high performance. A high pressure bearing must be able to withstand the large forces introduced into the structure as well as the higher thermal exertion. The bearing designed meet these requirements and demonstrates the advantages of another bearing arrangement. Due to the higher requirements it is more difficult to manufacture and more expensive then the bearing proposed in Chapter 5.

6.1 Design Considerations

A model design was realized using thin plates of 15 mm thickness containing the bearing geometry and straight fluid holes to supply and to recalculate the water. A drawing of the load bearing pad is shown in Appendix D. These plates are arranged around the bearing rail in a wrap around fashion. The fluid is distributed to the bearings via a multi-layer manifold. This manifold geometry fits ideally into the narrow gap between carriage and bearing rail allowing a modular design with an infinite number of opposed bearing pads along a carriage. The manifold does not need long holes since every layer contains one path, connecting two bearing opposed bearing pads in one flow direction, milled on its back. Stacked together they form a complete manifold supplying the fluid and connecting restrictor and bearing pads. Figure 6.1 shows the bearing arrangement in a wrap-around design.

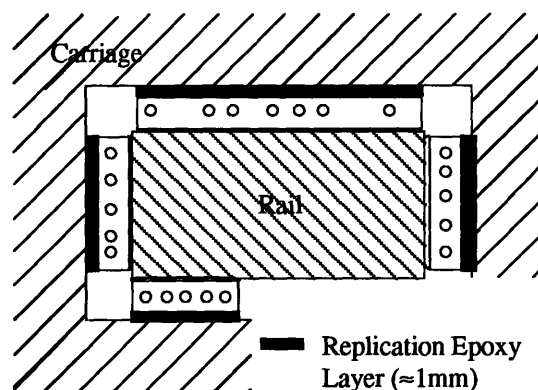


Figure 6.1: Bearing arrangement (wrap-around) of case study 2.

Now only constrained by the feasibility of the manifold the bearings can be arranged in every desired way. In the presented bearing one set of horizontal and one set of vertical bearings was ordered around one rail, while the remaining set of vertical bearings was ordered on the second rail. This allows the design to compensate for thermal expansions orthogonal to the direction of motion. Appendix D shows the implementation of the bearings around the rails and the manifolds. It should be noted, that there will be no tilting in the bearing due to the unequally sized bearing pads. Only the preload bearing pad could widen its bearing gap due to the force it exerts on the structure.



Figure 6.2: Ceramic test bearing.

All bearing components were made from aluminum oxide (Alumina), the base, the carriage and the bearings. Alumina has the thermal and dimensional stability required to withstand the high forces introduced into the system . It has an extreme high stiffness, a low coefficient of thermal expansion but also a low heat conductivity. This makes it favorable as a structural material. However, Aluminum provides nearly no damping and the low heat conductivity can lead to deformations in the structure. Combined with hydrostatic bearings and there high stiffness and damping levels, and means to introduce damping into the structure, Aluminum is a very favorable material. Furthermore the straightness level attainable with Alumina are excellent and it is resistant to water and most chemicals, i.e. an Alumina structure will not corrode. Aluminum for the rails as well as for the bearings

assures the bearings ability to withstand possible fluid breakdown without damage to the bearing.

6.2 Manufacturing

The manufacturing of ceramic components has become easier and cheaper in recent years. But compared with other materials, they are still expensive and difficult to manufacture. Therefore the entire carriage and base was designed from stock material. The bearing pads were custom designed and manufactured.

To assemble the bearing system the bearing pads are placed and aligned on the rails and the manifold connected to the bearing pads. An equal bearing gap is of 15 μm is assured by shim stock between bearing and rail .They are held on the rail by a vacuum applied to the bearing pads through the bearing supply hole. With all bearings in place the carriage is position above the bearing. Finally epoxy is injected into epoxy pockets on the back of the bearings fixing the bearings to the carriage. The greatest advantage of this assembly process is that even smaller bearing gaps can be realized without excessive precision processes and the associated cost.

6.3 Bearing design

Again, no direct requirements for the test bearing exist. The performance for the given supply pressure has to be optimized. The resulting choice in bearing geometry is shown below. In order to provide more damping additional squeeze film lands are incorporated into the bearing pocket shown in Appendix D.

<i>supply pressure</i>	<i>ps (atm, Pa= N/m²)</i>	20.41	2,067,857
	<i>ps (psi)</i>	300	
<i>dynamic viscosity</i>	<i>μ [mu] (Nsec/m²)</i>	Water	0.001
<i>pocket depth</i>	<i>hp (μm, m)</i>	300	0.000300
<i>nominal bearing gap</i>	<i>h (μm, m)</i>	15	0.000015
<i>bearing geometry:</i>			
<i>upper bearing pad:</i>			
<i>bearing width</i>	<i>au (mm, m)</i>	120	0.120
<i>bearing length</i>	<i>bu (mm, m)</i>	120	0.120
<i>land width</i>	<i>lu (mm, m)</i>	10	0.010

lower bearing pad:

<i>bearing width</i>	<i>al (mm, m)</i>	35	<i>0.035</i>
<i>bearing length</i>	<i>bl (mm, m)</i>	95	<i>0.095</i>
<i>land width</i>	<i>ll (mm, m)</i>	6	<i>0.006</i>

The calculated load capacity and stiffness values are, as expected, very high. The values are shown in Figure 6.3 and 6.4. It should also be noted that if lower stiffness and load capacity is required the lower supply should be increases, resulting in a bearing with minimum power requirements. The power and stiffness at zero displacement for different supply pressure of this bearing configuration with are shown in Figure 6.5 and 6.6.

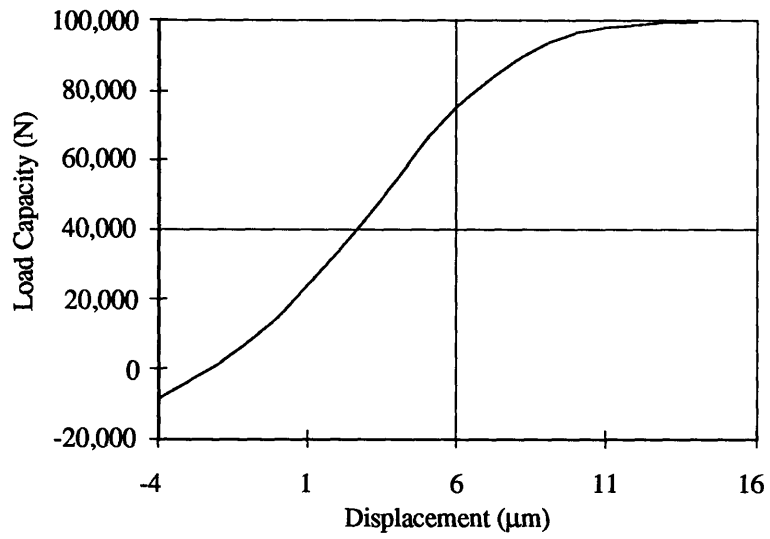


Figure 6.3: Load capacity of the high pressure bearing

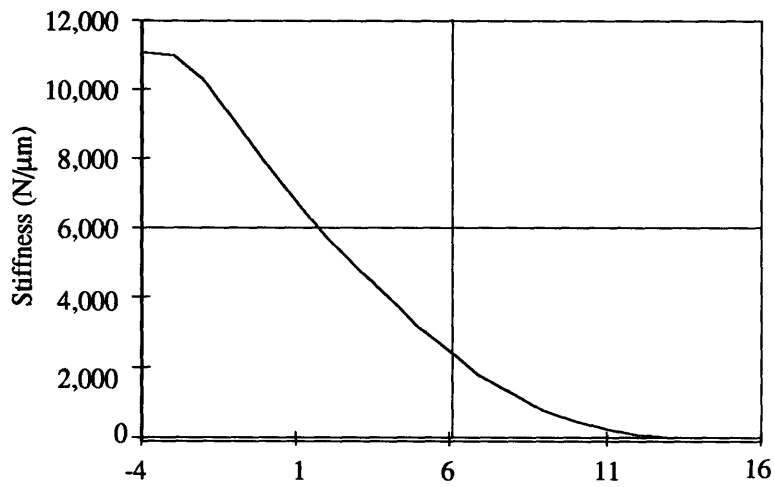


Figure 6.4: Stiffness of the high pressure bearing

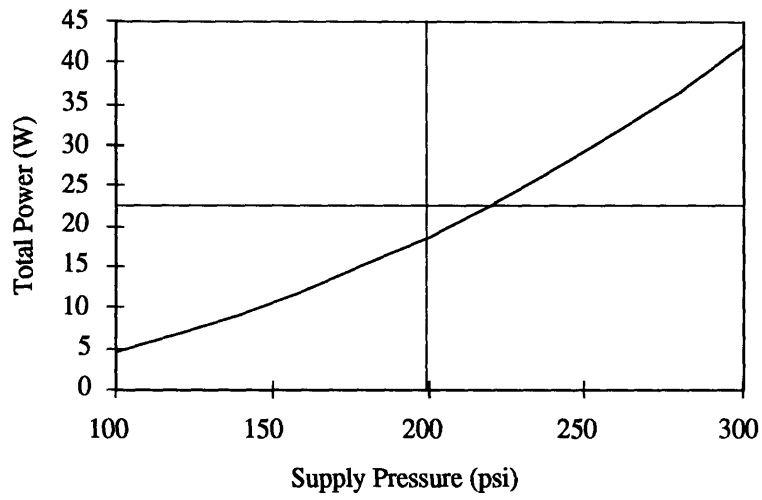


Figure 6.5: Total power as a function of supply pressure

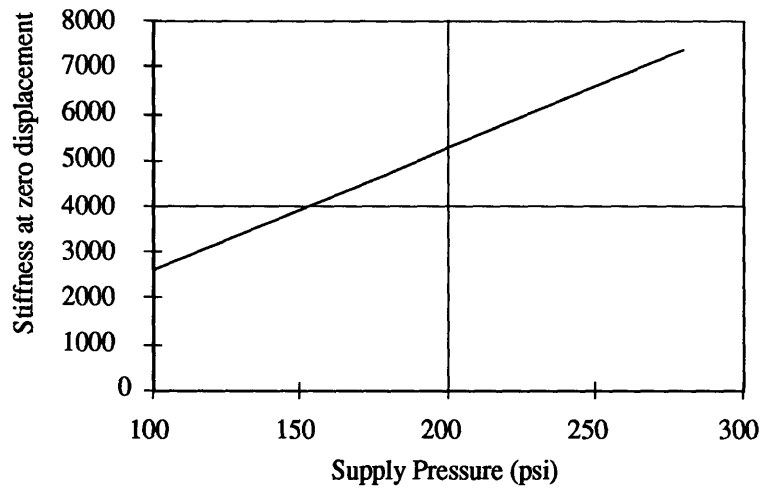


Figure 6.6: Stiffness at zero displacement as a function of supply pressure

7. Conclusion

An new type of hydrostatic bearing, Hydroguide™, applied to linear motion systems proved its excellent performance in terms of stiffness, load capacity and damping. It overcomes the disadvantages generally associated with this type of bearing. It is self-compensated and therefore self-cleaning. Since the smallest diameter passage is 3-5 mm it does not tend to clog. No last chance filter are necessary to operate the bearing reliable.

The performance can be predicted accurately since the flow pattern in the bearing and restrictor pads are deterministic. Using spreadsheet programs, the design of linear motion systems using Hydroguide™ is easy to apply and parameter studies performed show the possibilities and limits of design choices.

Water is used as bearing fluid providing a high heat capacity, high thermal conductivity and a low viscosity. In addition, water is environmentally friendly.

This bearing minimizes the disadvantages of hydrostatic bearings while increasing its performance. Decreased required pump power, higher reliability and its high performance make it a superior bearing for high precision applications in linear motion system as shown in both case studies presented.

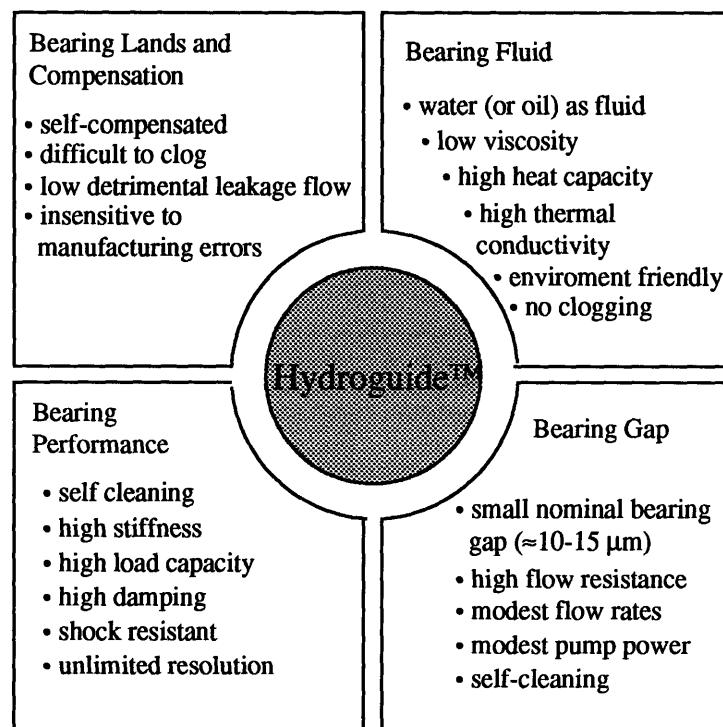


Figure 7.1: Properties of a self-compensated bearing

8. References

- [1], Alexander H. Slocum, **Precision Machine Design**, Prentice Hall, Englewood Cliffs, NJ, 1992.
- [2], Alexander H. Slocum, **Self Compensating Hydrostatic Bearing**, US Patent #5,104,237, April 14, 1992.
- [3], H.Gaub, **Hydrostatic Linear Motion Bearings for Precision Machine Tools**, MIT Master Thesis, 1992
- [4], Manfred Weck, **Werkzeugmaschinen und Fertigungssysteme**, Band 2, 4.Auflage, VDI-Verlag, Düsseldorf, 1991.
- [5], G. Pahl and W. Beitz, **Konstruktionslehre**, Springer Verlag, Berlin 1992.
- [6], W. Rowe, **Hydrostatic and Hybrid Bearing Design**, Butterworth, London, 1983.
- [7], F. Stansfield, **Hydrostatic Bearings for Machine Tools**, Machinery Publishing Co., Ltd., London, 1970.
- [8], D. Fuller, **Theory and Practice of Lubrication for Engineers**, 2nd ed., John Wiley & Sons, New York, 1984.
- [9], R. Schönfeld, “**Steife und Dämpfung hydrostatischer Führungen verbessern**”, *Werkstatt und Betrieb* 122 (1989) 1, p. 971-974.
- [10], R.S. Hahn, **Some Advantages of Hydrostatic Bearings in Machine Tools**, *Lubrication Engineering*, Vol. 21, No. 3, March 1965, pp. 89-96
- [11], T. Viersma, **Synthesis and Design of Hydraulic Systems and Pipelines**, Elsevier Scientific Publishing Company, Amsterdam, 1980.
- [12], J. A. Fay, **Introduction to Fluid Mechanics**, Lecture notes of Mitt's 'Advanced Fluid Mechanics' course, Cambridge, 1993.
- [13], D. E. Newland, **Random Vibrations and Spectral Analysis**, Wiley, 1984.
- [14], R. B. Randall, **Frequency Analysis**, Brüel and Kjær, 1987.
- [15], A. G. Piersol, J. S. Bendat, **Random Data: Analysis and Measurement**, Wiley, 1986.

9. Appendices

9.1. Appendix A: Spreadsheet for Case Study 1

Spreadsheet for the Hydroguide™

Precision Engineering Research Group

Massachusetts Institute of Technology

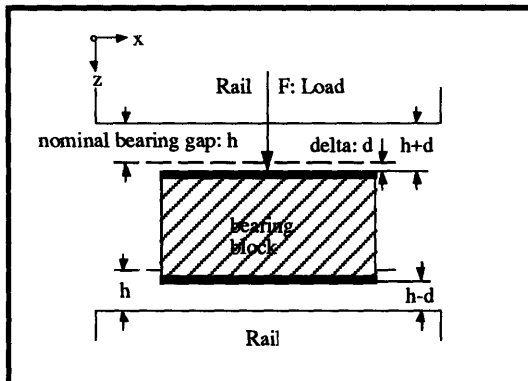
(last revised version, 1. December 1993)

Input:

General Input:

supply pressure	ps (atm, Pa= N/m ²)	1.3606	137,863
	ps (psi)	20.00082	
dynamic viscosity	μ [mu] (Nsec/m ²)	0.001	
density ρ	rho (kg/m ³)	997	
pocket depth	hp (μ m, m)	300	0.000300
nominal bearing gap	h (μ m, m)	15	0.000015
first deviation from nominal gap	del (μ m, m)	1.5	0.0000015
second deviation from nominal gap	dels (μ m, m)	3.8	3.78348E-06
negative second deviation from nominal gap	ndels (μ m, m)	-3.8	-3.78348E-06
angle between rail surfaces and horizontal	alpha (degrees)	0	
carriage weight	wc[N]	100	

- *Positive displacement (deviation from nominal bearing gap) is defined as decrease of the load bearing gap in response to a positive load.*
- *stiffness is defined as change in the bearing gap in response to a varying load.*



- *Assign a location for the bearing pads according to the definition of positive displacement.*
- *Remember, the load bearing pads gap decreases when a positive load is applied.*

load bearing pad:	(upper or lower)	upper
preload bearing pad:	(upper or lower)	lower

bearing geometry:**upper bearing pad:**

bearing width	au (mm, m)	110	0.110
bearing length	bu (mm, m)	110	0.110
land width	lu (mm, m)	15	0.015
pocket radius	rpu (mm, m)	5	0.005
effective bearing pad area	AAu (mm ² , m ²)	8825	0.008825
flow resistance:			
at delta=0	Rbu (Nsec/m ⁵)	1.53E+11	
at first displacement delta	Rbud (Nsec/m ⁵)	2.10E+11	
at second displacement delta	Rbuds (Nsec/m ⁵)	3.67E+11	
at second negative displacement delta	mRbuds (Nsec/m ⁵)	7.81E+10	

lower bearing pad:

bearing width	al (mm, m)	45	0.045
bearing length	bl (mm, m)	90	0.090
land width	ll (mm, m)	10	0.010
pocket radius	rpl (mm, m)	5	0.005
effective bearing pad area	AAI (mm ² , m ²)	2686	0.002686
flow resistance			
at delta=0	Rbl (Nsec/m ⁵)	1.72E+11	
at first displacement delta	Rbld (Nsec/m ⁵)	1.29E+11	
at second displacement delta	Rbls (Nsec/m ⁵)	8.74E+10	
at second negative displacement delta	mRbls (Nsec/m ⁵)	4.10E+11	

Input 1 (set input 2 to 0)

•Using input 1 for calculations requires to set input 2 to zero

•For gamma 1 and gamma 2 (k1, k2) input a 1 and use it as an initial value for later optimization

Restrictor resistance ratio:

for upper flow restrictor $k1=Rur/Rlb$ (gam1) **2.88**

for lower flow restrictor $k2=Rlr/Rub$ (gam2) **3.22**

desired flow resistance:

for upper restrictor Rru, des (Nsec/m⁵) **4.93E+11**

for lower restrictor Rrl, des (Nsec/m⁵) **4.93E+11**

required collector length:

for upper flow restrictor pad cl (mm, m) **2.00** 0.0020

for lower flow restrictor pad cl (mm, m) **2.00** 0.0020

Input 2 (set input 1 to 0)

•Using input 2 for calculations requires to set input 1 to zero

•The restrictor pad geometry including the override dimension is shown in Figure 3

Collector length override:

for upper flow restrictor oru (mm,m) **0**

for lower flow restrictor orl (mm,m) **0**

Restrictor resistance ratio for upper flow restrictor pad (input 2):

for upper flow restrictor pad	$k1=Rur/Rlb$ (gam1)		
for lower flow restrictor pad	$k2=Rlr/Rub$ (gam2)		
upper flow restrictor pad			
(for lower bearing pad):			
supply groove width	usgw (mm, m)	6.00	0.0060
restrictor land width	urlw (mm, m)	5.00	0.0050
collector groove width	ucgw (mm, m)	6.00	0.0060
supply groove axial offset for larger port	usgo (mm, m)	0.00	0.0000
flow resistance of round end portions	(Nsec/m ⁵)	5.55E+11	
required flow resistance of linear portion	(Nsec/m ⁵)	4.45E+12	
collector length	cl (mm, m)	2.00	0.0020
flow resistance at delta=0	Rru (Nsec/m ⁵)	4.93E+11	
flow resistance at first displacement delta	Rrud (Nsec/m ⁵)	6.77E+11	
flow resistance at 2nd displacement delta	Rruds (Nsec/m ⁵)	1.18E+12	
flow resistance at -2nd displacement delta	mRruds (Nsec/m ⁵)	2.51E+11	
annular groove outer radius	uagr (mm, m)	14.00	0.0140
leakage land radius	ullr (mm, m)	29.00	0.0290
leakage land width	ullw (mm, m)	15.00	0.0150
Total compensator length	(mm, m)	60.00	
leakage resistance from rounded ends	(Nsec/m ⁵)	4.12E+11	
leakage resistance from linear region	(Nsec/m ⁵)	1.33E+13	
leakage resistance at delta=0	Rlu (Nsec/m ⁵)	4.00E+11	
leakage resistance at displacement delta	Rlud (Nsec/m ⁵)	5.48E+11	
	Rlu/Rru	0.81	
lower flow restrictor pad			
(for upper bearing pad):			
supply groove width	lsgw (mm, m)	6.00	0.0060
restrictor land width	lrlw (mm, m)	5.00	0.0050
collector groove width	lcgw (mm, m)	6.00	0.0060
supply groove axial offset for larger port	lsgo (mm, m)	0.00	0.0000
flow resistance of round end portions	(Nsec/m ⁵)	5.55E+11	
required flow resistance of linear portion	(Nsec/m ⁵)	4.44E+12	
collector length	cl (mm, m)	2.00	0.0020
flow resistance at delta=0	Rrl (Nsec/m ⁵)	4.93E+11	
flow resistance at first displacement delta	Rrld (Nsec/m ⁵)	3.71E+11	
flow resistance at 2nd displacement delta	Rrlds (Nsec/m ⁵)	2.51E+11	
flow resistance at -2nd displacement delta	mRrlds (Nsec/m ⁵)	1.18E+12	
annular groove outer radius	lagr (mm, m)	14.00	0.0140
leakage land radius	lllr (mm, m)	29.00	0.0290
leakage land width	lllw (mm, m)	15.00	0.0150
Total compensator length	(mm, m)	60.00	
leakage resistance from rounded ends	(Nsec/m ⁵)	4.12E+11	
leakage resistance from linear region	(Nsec/m ⁵)	1.33E+13	
leakage resistance at delta=0	Rll (Nsec/m ⁵)	4.00E+11	

leakage resistance at displacement delta	Rlld (Nsec/m ⁵)	3.00E+11	
	Rll/Rrl	0.81	
Pocket pressures:			
pocket pressure:			
pocket pressure in upper bearing pad			
at delta=0	ppu (atm, Pa=N/m ²)	0.32	32,674
at first displacement delta	ppud (atm, Pa=N/m ²)	0.49	49,891
at second displacement delta	ppuds (atm, Pa=N/m ²)	0.81	81,792
at minus second displacement delta	mppuds (atm, Pa=N/m ²)	0.08	8,553
pocket pressure in lower bearing pad			
at delta=0	ppl (atm, Pa=N/m ²)	0.35	35,574
at first displacement delta	ppld (atm, Pa=N/m ²)	0.22	22,058
at second displacement delta	pplds (atm, Pa=N/m ²)	0.09	9,505
at minus second displacement delta	mpplds (atm, Pa=N/m ²)	0.84	85,508
Maximum velocity (with no pre-feed)			
avg. flow velocity out of pocket	(m/s, m/min)	0.03	2
	(ipm)	76.30	
table velocity	(m/s, m/min)	0.50	30
max. velocity so inflow = 0.75 outflow	(m/s, m/min)	0.05	3
	(ipm)	114.45	
Load carrying efficiency			
load efficiency (Fmax/(P*A))		42%	
Flow and pump power			
total fluid flow per pad pair	Q (l/min)	0.07	
total fluid flow	Q (l/min)	0.27	
total pump power	P (W)	0.15	
total shear power at max velocity	Pshear (W)	0.01	
total power of the system	Ptotal (W)	0.16	
power ratio	K	0.04	
displacement at 0 load	(m)	2.25E-06	
Total fluid flow	Q [l/min]	0.27	
Total pump power	P (W)	0.00	
table velocity	(m/sec,m/min)	0.5	30
pocket reynolds number	mump	149.55	

load capacity and stiffness

per bearing block

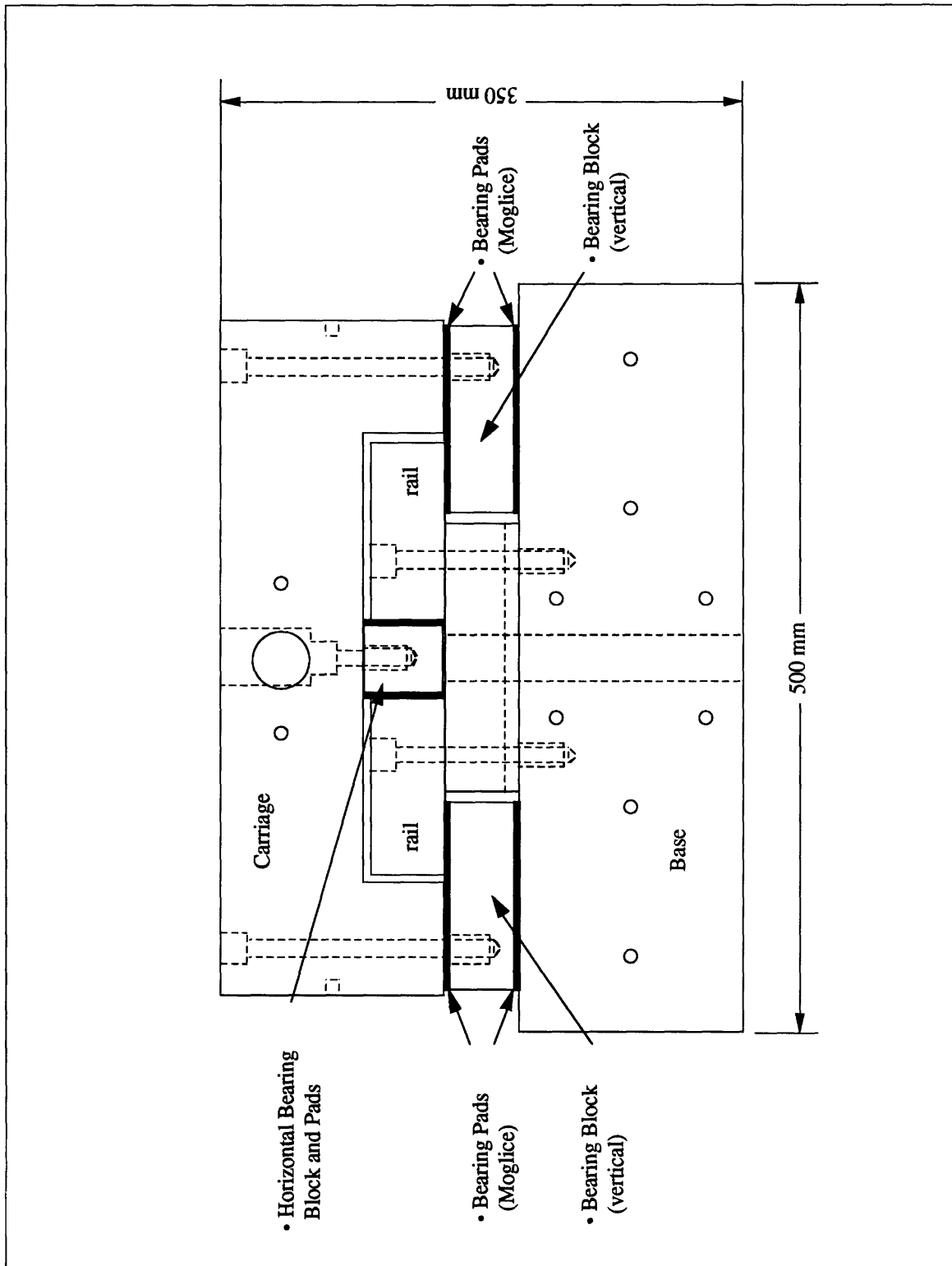
displacement	(%)	0	10	25.22	-25.22
smallest gap	(μm)	15	13.5	11.21	11.21
load capacity	F (N)	193	381	696	-154
	F (N)	193	381	696	-154
	F (lbf)	43	86	156	-35
stiffness	(N/ μm)	116	97	68	136
	(lbf/ μin)	0.7	0.6	0.4	0.8

for the system:

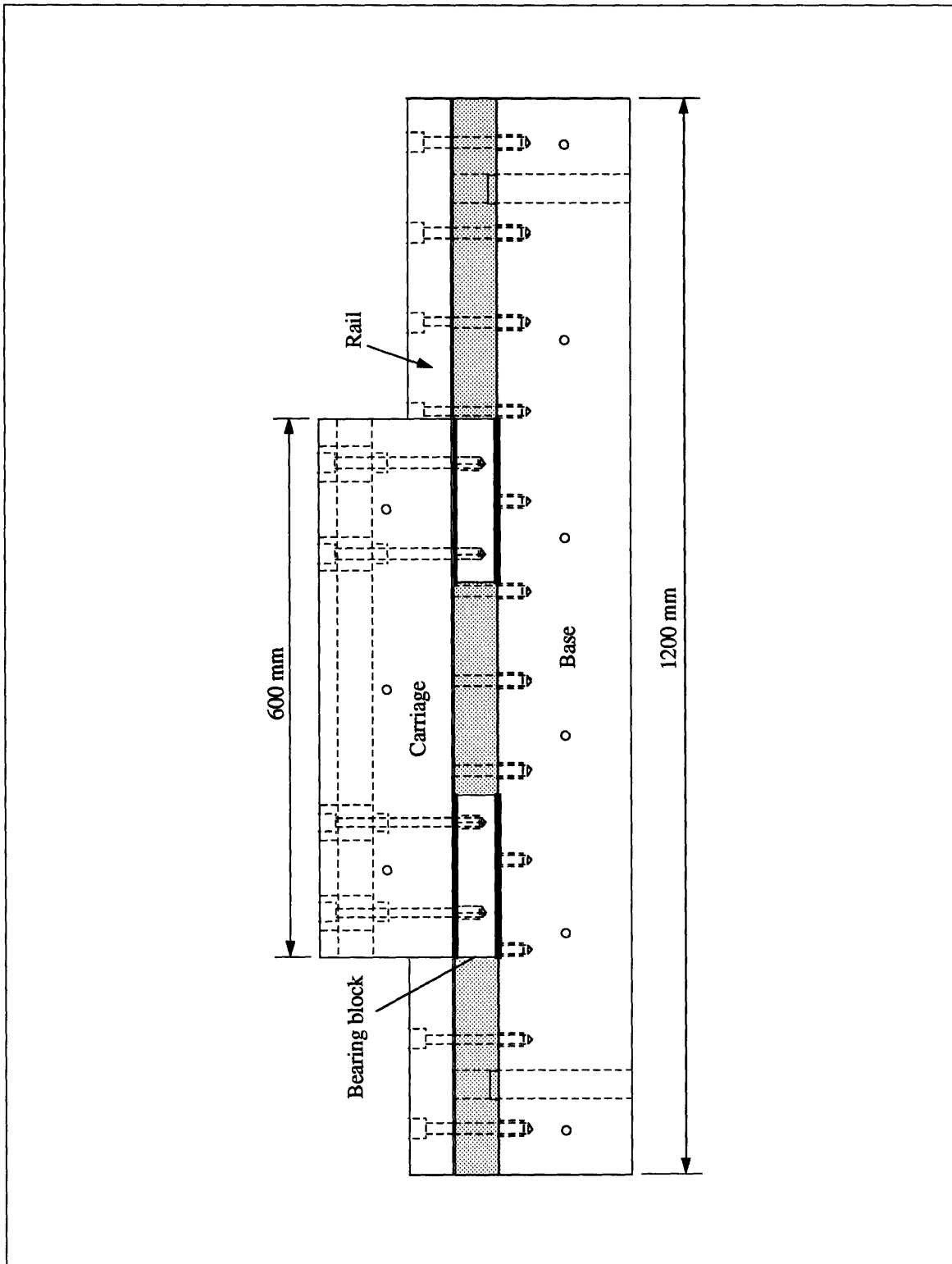
number of bearing blocks **4**

displacement	(%)	0	10	25.22	-25.22
smallest gap	(μm)	15	13.5	11.21	11.21
load capacity	F (N)	771.16	1524.13	2785.12	-616.78
	F (lbf)	173.30	342.50	625.87	-138.60
stiffness	(N/ μm)	465.44	386.47	270.00	542.24
	(lbf/ μin)	2.66	2.21	1.54	3.10

9.2 Appendix B: Mechanical Drawings for Case Study 1



9.2 Appendix B: Mechanical Drawings for Case Study 1



Input 2 (set input 1 to 0)

•Using input 2 for calculations requires to set input 1 to zero

•The restrictor pad geometry including the override dimension is shown in Figure 3

Collector length override:

for upper flow restrictor	oru (mm,m)	0
for lower flow restrictor	orl (mm,m)	0
Restrictor resistance ratio for upper flow restrictor pad (input 2):		
for upper flow restrictor pad	k1=Rur/Rlb (gam1)	
for lower flow restrictor pad	k2=Rlr/Rub (gam2)	

**upper flow restrictor pad
(for lower bearing pad):**

supply groove width	usgw (mm, m)	2.50	0.0025
restrictor land width	urlw (mm, m)	4.00	0.0040
collector groove width	ucgw (mm, m)	4.00	0.0040
supply groove axial offset for larger port	usgo (mm, m)	0.00	0.0000
flow resistance of round end portions	(Nsec/m ⁵)	6.22E+11	
required flow resistance of linear portion	(Nsec/m ⁵)	5.69E+11	
collector length	cl (mm, m)	12.50	0.0125
flow resistance at delta=0	Rru (Nsec/m ⁵)	2.97E+11	
flow resistance at first displacement delta	Rrud (Nsec/m ⁵)	4.07E+11	
flow resistance at 2nd displacement delta	Rruds (Nsec/m ⁵)	5.80E+11	
flow resistance at -2nd displacement delta	mRruds (Nsec/m ⁵)	1.72E+11	
annular groove outer radius	uagr (mm, m)	8.50	0.0085
leakage land radius	ullr (mm, m)	23.50	0.0235
leakage land width	ullw (mm, m)	15.00	0.0150
Total compensator length	(mm, m)	59.50	
leakage resistance from rounded ends	(Nsec/m ⁵)	5.75E+11	
leakage resistance from linear region	(Nsec/m ⁵)	2.13E+12	
leakage resistance at delta=0	Rlu (Nsec/m ⁵)	4.53E+11	
leakage resistance at displacement delta	Rlud (Nsec/m ⁵)	6.22E+11	
	Rlu/Rru	1.53	

bearing geometry:**upper bearing pad:**

bearing width	au (mm, m)	120	0.120
bearing length	bu (mm, m)	120	0.120
land width	lu (mm, m)	10	0.010
pocket radius	rpu (mm, m)	5	0.005
effective bearing pad area	AAu (mm ² , m ²)	11986	0.011986
flow resistance:			
at delta=0	Rbu (Nsec/m ⁵)	8.52E+10	
at first displacement delta	Rbud (Nsec/m ⁵)	1.17E+11	
at second displacement delta	Rbuds (Nsec/m ⁵)	1.66E+11	
at second negative displacement delta	mRbuds (Nsec/m ⁵)	4.93E+10	

lower bearing pad:

bearing width	al (mm, m)	35	0.035
bearing length	bl (mm, m)	95	0.095
land width	ll (mm, m)	6	0.006
pocket radius	rpl (mm, m)	5	0.005
effective bearing pad area	AAI (mm ² , m ²)	2516	0.002516
flow resistance			
at delta=0	Rbl (Nsec/m ⁵)	9.71E+10	
at first displacement delta	Rbld (Nsec/m ⁵)	7.29E+10	
at second displacement delta	Rbls (Nsec/m ⁵)	5.62E+10	
at second negative displacement delta	mRbls (Nsec/m ⁵)	1.90E+11	

Input 1 (set input 2 to 0)

•Using input 1 for calculations requires to set input 2 to zero

•For gamma 1 and gamma 2 (k1, k2) input a 1 and use it as an initial value for later optimization

Restrictor resistance ratio:

for upper flow restrictor	k1=Rur/Rlb (gam1)	3.06	
for ower flow restrictor	k2=Rlr/Rub (gam2)	4.01	
desired flow resistance:			
for upper restrictor	Rru, des (Nsec/m ⁵)	2.97E+11	
for lower restrictor	Rrl, des (Nsec/m ⁵)	3.42E+11	
required collector length:			
for upper flow restrictor pad	c1 (mm, m)	12.50	0.0125
for lower flow restrictor pad	c1 (mm, m)	8.00	0.0080

9.3 Appendix C: Spreadsheet for Case Study 2

Spreadsheet for the Hydroguide™

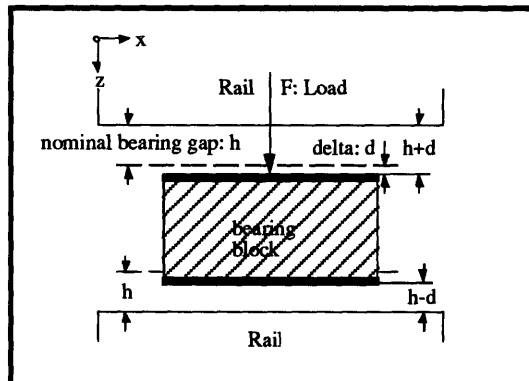
Precision Engineering Research Group
 Massachusetts Institute of Technology
 (last revised version, 1. December 1993)

Input:

General Input:

supply pressure	ps (atm, Pa= N/m ²)	20.41	2,067,857
	ps (psi)	300	
dynamic viscosity	μ [mu] (Nsec/m ²)	0.001	
density ρ	rho (kg/m ³)	997	
pocket depth	hp (μ m, m)	300	0.000300
nominal bearing gap	h (μ m, m)	15	0.000015
first deviation from nominal gap	del (μ m, m)	1.5	0.0000015
second deviation from nominal gap	dels (μ m, m)	3.0	0.000003
negative second deviation from nominal gap	ndels (μ m, m)	-3.0	-0.000003
angle between rail surfaces and horizontal	alpha (degrees)	0	
carriage weight	wc[N]	100	

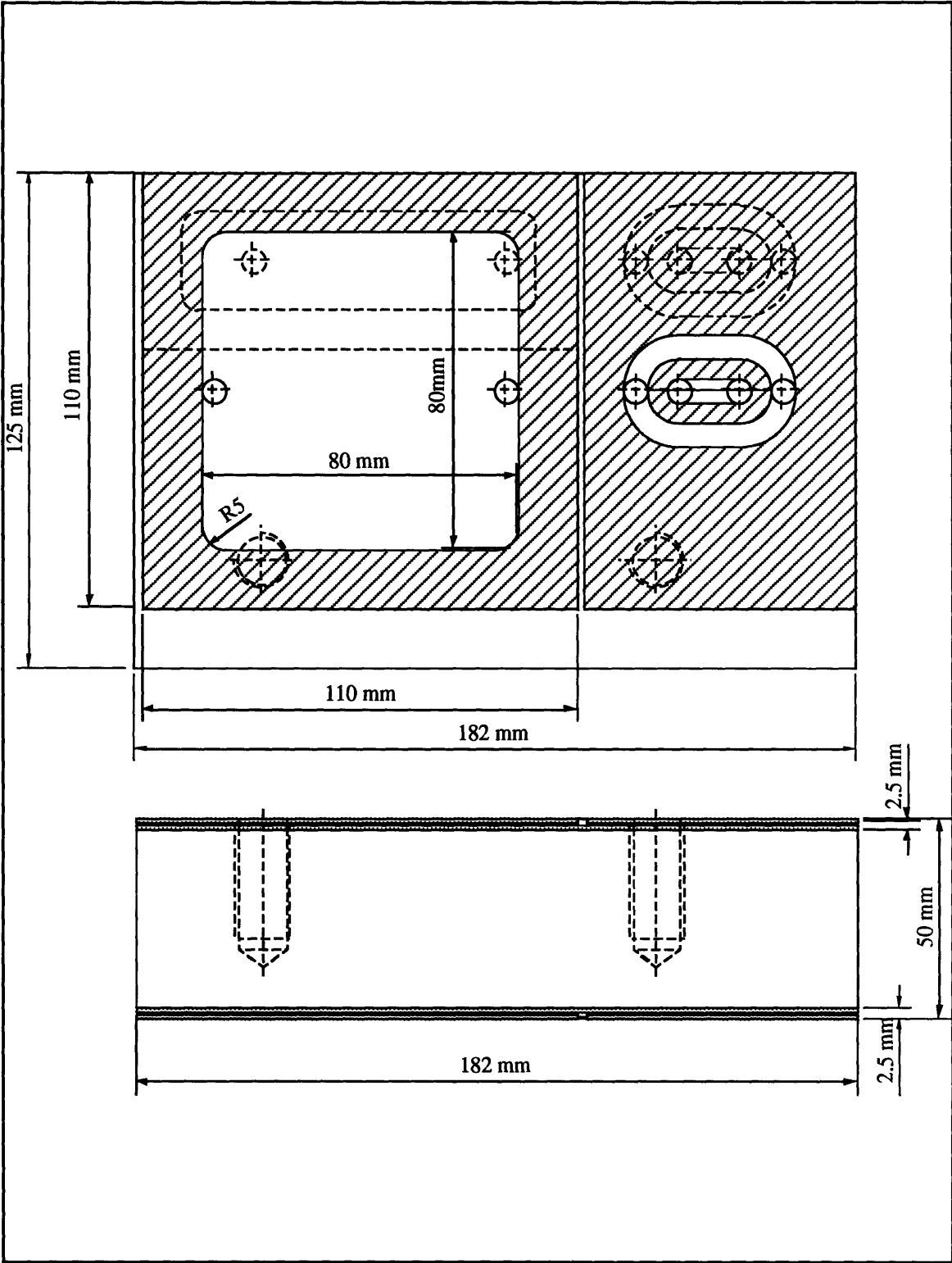
- *Positive displacement (deviation from nominal bearing gap) is defined as decrease of the load bearing gap in response to a positive load.*
- *stiffness is defined as change in the bearing gap in response to a varying load.*



- *Assign a location for the bearing pads according to the definition of positive displacement.*
- *Remember, the load bearing pads gap decreases when a positive load is applied.*

load bearing pad: (upper or lower) **upper**
 preload bearing pad: (upper or lower) **lower**

9.2 Appendix B: Mechanical Drawings for Case Study 1



**lower flow restrictor pad
(for upper bearing pad):**

supply groove width	lsgw (mm, m)	6.00	0.0060
restrictor land width	lrlw (mm, m)	5.00	0.0050
collector groove width	lsgw (mm, m)	6.00	0.0060
supply groove axial offset for larger port	lsgo (mm, m)	0.00	0.0000
flow resistance of round end portions	(Nsec/m ⁵)	5.55E+11	
required flow resistance of linear portion	(Nsec/m ⁵)	8.89E+11	
collector length	cl (mm, m)	8.00	0.0080
flow resistance at delta=0	Rrl (Nsec/m ⁵)	3.70E+11	
flow resistance at first displacement delta	Rrld (Nsec/m ⁵)	2.78E+11	
flow resistance at 2nd displacement delta	Rrlds (Nsec/m ⁵)	2.14E+11	
flow resistance at -2nd displacement delta	mRrlds (Nsec/m ⁵)	7.23E+11	
annular groove outer radius	lagr (mm, m)	8.50	0.0140
leakage land radius	lllr (mm, m)	29.00	0.0290
leakage land width	lllw (mm, m)	20.50	0.0205
Total compensator length	(mm, m)	66.00	
leakage resistance from rounded ends	(Nsec/m ⁵)	4.12E+11	
leakage resistance from linear region	(Nsec/m ⁵)	3.33E+12	
leakage resistance at delta=0	Rll (Nsec/m ⁵)	3.67E+11	
leakage resistance at displacement delta	Rlld (Nsec/m ⁵)	2.76E+11	
	Rll/Rrl	0.99	

Pocket pressures:

pocket pressure:

pocket pressure in upper bearing pad

at delta=0	ppu (atm, Pa=N/m ²)	3.82	387,020
at first displacement delta	ppud (atm, Pa=N/m ²)	6.04	612,025
at second displacement delta	ppuds (atm, Pa=N/m ²)	8.92	904,249
at minus second displacement delta	mppuds (atm, Pa=N/m ²)	1.30	132,066

pocket pressure in lower bearing pad

at delta=0	ppl (atm, Pa=N/m ²)	5.03	509,222
at first displacement delta	ppld (atm, Pa=N/m ²)	3.10	313,863
at second displacement delta	pplds (atm, Pa=N/m ²)	1.80	182,507
at minus second displacement delta	mpplds (atm, Pa=N/m ²)	10.70	1,084,403

Maximum velocity (with no pre-feed)

avg. flow velocity out of pocket	(m/s, m/min)	0.63	38
	(ipm)	1489.86	
table velocity	(m/s, m/min)	0.50	30
max. velocity so inflow = 0.75 outflow	(m/s, m/min)	0.95	57
	(ipm)	2234.79	

Load carrying efficiency

load efficiency (Fmax/(P*A)) 35%

Flow and pump power

total fluid flow per pad pair	Q (l/min)	1.22
total fluid flow	Q (l/min)	4.89
total pump power	P (W)	42.12
total shear power at max velocity	Pshear (W)	2.01
total power of the system	Ptotal (W)	44.14
power ratio	K	0.05

displacement at 0 load	(m)	2.25E-06
Total fluid flow	Q [l/min]	4.89
Total pump power	P (W)	0.00

table velocity	(m/sec,m/min)	0.5
pocket reynolds number	mump	149.55

30

load capacity and stiffness

per bearing block

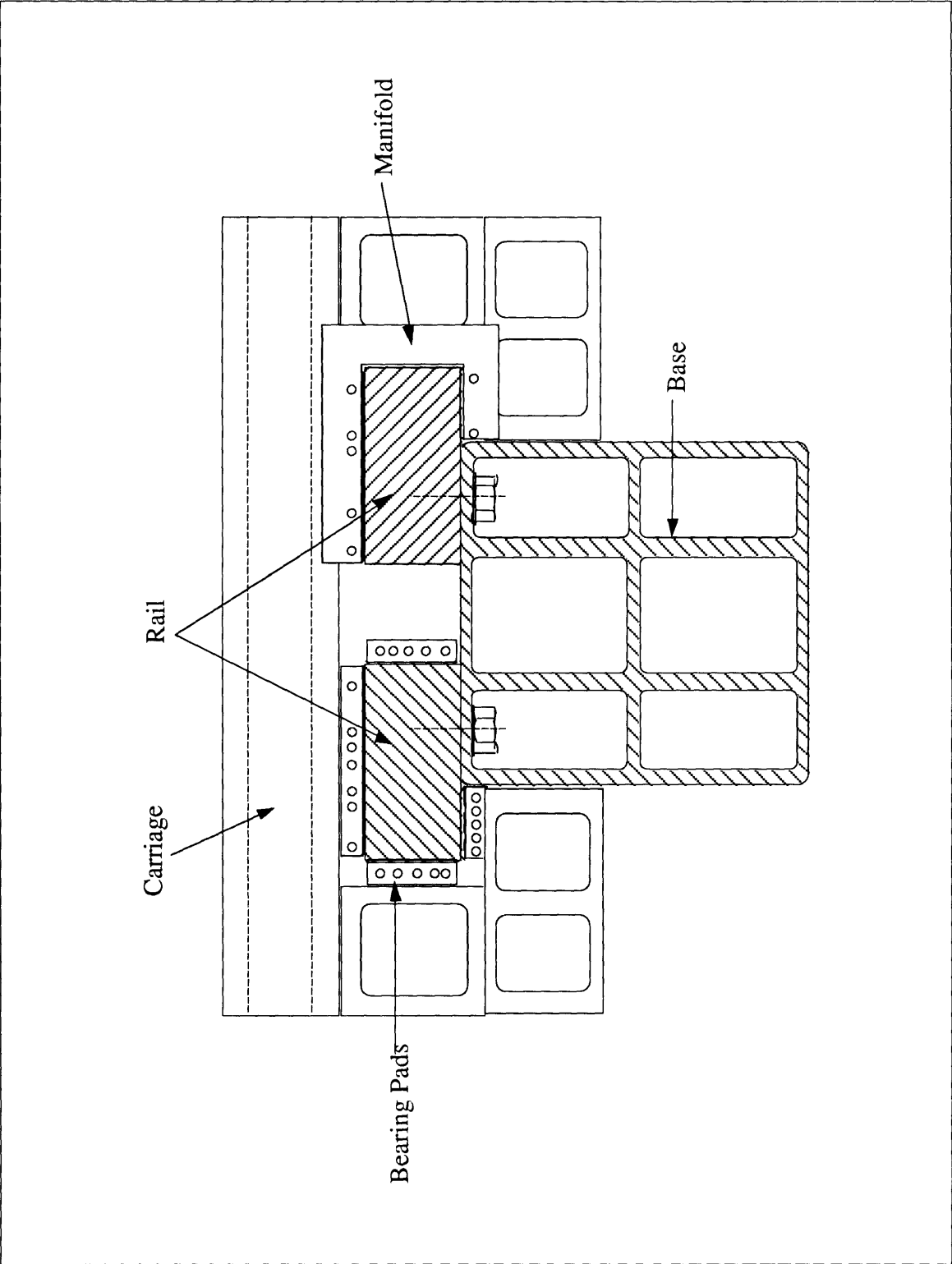
displacement	(%)	0	10	20	-20
smallest gap	(μm)	15	13.5	12	12
load capacity	F (N)	3,667	6,966	10,869	-1,023
	F (N)	3,357	6,546	10379	-1146
	F (lbf)	824	1,565	2,442	-230
stiffness	(N/ μm)	1970	1551	1203	2737
	(lbf/ μin)	11.3	8.9	6.9	15.6

for the system:

number of bearing blocks 4

displacement	(%)	0	10	20	-20
smallest gap	(μm)	15	13.5	12	12
load capacity	F (N)	14666.68	27862.84	43476.50	-4091.74
	F (lbf)	3295.88	6261.31	9770.00	-919.49
stiffness	(N/ μm)	7881.61	6203.97	4810.05	10948.86
	(lbf/ μin)	45.04	35.45	27.49	62.56

9.4 Appendix D: Mechanical Drawings for Case Study 2



9.4 Appendix D: Mechanical Drawings for Case Study 2

